NOVA SCHOOL OF SCIENCE & TECHNOLOGY

DEPARTAMENT OF MECHANICAL AND INDUSTRIAL ENGINEERING

VASCO DE FIGUEIREDO NUNES

Graduate in Sciences of Mechanical Engineering

FRICTION ROLLING ADDITIVE MANUFACTURING: PROCESS IMPLEMENTATION AND FEASIBILITY STUDY OF CERAMIC PARTICLE INCORPORATION

INTEGRATED MASTER IN MECHANICAL ENGINEERING

Universidade NOVA de Lisboa

September, 2024

DEPARTAMENT OF MECHANICAL
AND INDUSTRIAL ENGINEERING

FRICTION ROLLING ADDITIVE MANUFACTURING: PROCESS IMPLEMENTATION AND FEASIBILITY STUDY OF CERAMIC PARTI-CLE INCORPORATION

VASCO DE FIGUEIREDO NUNES

Graduate in Sciences of Mechanical Engineering

Adviser: Doctor Miguel Araújo Machado
Assistant Professor, Universidade NOVA de Lisboa

Co-advisers: Doctor Valdemar Rebelo Duarte
Invited Assistant Professor, Universidade NOVA de Lisboa

Examination Committee:

Chair: Doctor Carla Maria Moreira Machado,
Assistant Professor, FCT-NOVA

Rapporteurs: Doctor Catarina Isabel Silva Vidal,
Assistant Professor, FCT-NOVA
Doctor Pedro Daniel Marques Ferreira,
Invited Adjunct Professor, Instituto Politécnico de Setúbal

Adviser: Doctor Miguel Araújo Machado
Assistant Professor, Universidade NOVA de Lisboa

INTEGRATED MASTER IN MECHANICAL ENGINEERING

Universidade NOVA de Lisboa
September, 2024

Friction Rolling Additive Manufacturing: Process Implementation and Feasibility Study of Ceramic Particle Incorporation

ACKNOWLEDGMENTS

First, I would like to express my profound gratitude my supervisor and co-supervisor, Professor Dr. Miguel Machado and Professor Dr. Valdemar Duarte, for the opportunity to develop this innovative project, for their availability, guidance, assistance, and shared knowledge throughout this dissertation journey.

To Mr. António Campos and Mr. Paulo Magalhães for their unwavering support in the laboratories during the experimental work and they kind way of helping (kinda).

A word of thanks to my colleagues in the department, Engineer Rui, Engineer Werley, and Engineer Paulo for their endless willingness to assist in various phases of the experimental work and analysis.

To my lifelong companion (future Engineer) Ricardo Costa, for all the companionship, support, fun, and knowledge shared during these five years of work.

To my "compincha", Engineer Pedro Melo, for all the crazy conversations about life, for never letting me down, not just as a course mate or team member, but above all, as a great friend.

To my Inês, for always showing me clarity in the path to follow, for her patience, and for being there whenever I needed her most.

To my friends from college, I sincerely thank you for all the help throughout this journey. To my mental refuge, basketball, and to all my friends who made it even better, thank you for all the escapes from reality.

To my brother, for always helping me whenever I needed it, for being present in both my personal and academic life.

To my grandmother, in my heart, who has always been there for everything I needed during this academic and personal journey, for her concern and care.

Finally, to my parents, for always allowing me to carve my own path and for providing me with this leap in life that they cared so much about. "Já está!".

"O valor das coisas
não está no tempo
que elas duram,
mas na intensidade
com que acontecem.

Por isso existem
momentos inesquecíveis,
coisas inexplicáveis
e pessoas incomparáveis.
(Fernando Pessoa).

ABSTRACT

The development of the Friction Rolling Additive Manufacturing (FRAM) process was driven by the challenges of processing aluminum alloys in additive manufacturing (AM), particularly the solidification defects that can compromise part integrity. Conventional AM techniques that rely on material fusion struggle to produce high-strength aluminum alloys, highlighting the need for solid-state alternatives. FRAM provides an innovative solution by generating heat through friction, enabling the deposition of metallic materials in a solid state and thereby minimizing the risk of solidification defects. The primary objectives of this work were to establish the laboratory conditions necessary for the FRAM process for solid-state metals and to evaluate the feasibility of incorporating ceramic particles into the deposited metal layers. This involved the production of the friction tool, fine-tuning of operational parameters, and the development of a continuous guiding system for the feed material. Experimental tests were conducted to deposit aluminum layers with and without integrated ceramic particles, followed by characterization through tensile tests, hardness tests, and microstructural analyses.

Results showed that particle dispersion depends on the deposition parameters. Tensile tests revealed that particle presence did not affect the tensile strength, supporting the potential of composite fabrication via additive manufacturing. Hardness tests identified variations in areas where bonding occurred, forming a microstructure with distinct characteristics. The results indicated that the FRAM process has significant potential for producing metal matrix composites containing ceramic particles. However, challenges related to achieving uniform particle distribution and controlling process parameters remain to be addressed.

Keywords: Additive Manufacturing, Ceramic particles incoporation, FRAM, Metal matrix composite

RESUMO

O desenvolvimento do processo de *Friction Rolling Additive Manufacturing* (FRAM) foi motivado pelos desafios no processamento de ligas de alumínio no fabrico aditivo (FA), particularmente pelos defeitos de solidificação que podem comprometer a integridade das peças. As técnicas convencionais de FA, que dependem da fusão de materiais, têm dificuldades em produzir ligas de alumínio de elevada resistência, evidenciando a necessidade de alternativas em estado sólido. O processo FRAM oferece uma solução inovadora ao gerar calor por fricção, permitindo a deposição de materiais metálicos em estado sólido e, assim, minimizando o risco de defeitos de solidificação.

Os principais objetivos deste trabalho foram estabelecer as condições laboratoriais necessárias para o processo FRAM para metais em estado sólido e avaliar a viabilidade da incorporação de partículas cerâmicas nas camadas de metal depositadas. Isto envolveu a produção da ferramenta de fricção, o ajuste dos parâmetros operacionais e o desenvolvimento de um sistema de alimentação guiada contínua para o material de alimentação. Foram realizados testes experimentais para depositar camadas de alumínio com e sem partículas cerâmicas integradas, seguidos por caracterizações através de ensaios de tração, testes de dureza e análises microestruturais.

Os resultados mostraram que a dispersão de partículas depende dos parâmetros de deposição. Os ensaios de tração revelaram que a presença de partículas não afetou a resistência à tração, reforçando o potencial do fabrico de compósitos através do fabrico aditivo. Os ensaios de dureza identificaram variações nas áreas onde ocorreu a união, formando uma microestrutura com características distintas. Os resultados indicaram que o processo FRAM tem um potencial significativo para a produção de compósitos de matriz metálica contendo partículas cerâmicas. No entanto, desafios relacionados com a obtenção de uma distribuição uniforme das partículas e o controlo dos parâmetros do processo ainda precisam de ser resolvidos.

Palavras chave: Compósitos de Matriz Metálica, Fabrico Aditivo, FRAM, Incorporação de partículas cerâmicas

CONTENTS

LIST OF FIGURES

LIST OF TABLES

ACRONYMS

AFSD	Additive Friction Stir Deposition
AM	Additive Manufacturing.
DED	Directed Energy Deposition
EBSD	Electron Backscatter Diffraction
FRAM	Friction Rolling Additive Manufacturing.
FSAM	Friction Stir Additive Manufacturing
FSP	Friction Stir Processing
FSW	Friction Stir Welding
IS	International System
MMC	Metal Matrix Composites
OM	Optical Microscopy
PBF	Powder Bed Fusion
SEM	Scanning Electron Microscopy
UTS	Ultimate Tensile Strength
UFSP	Upward Friction Stir Processing
YS	Yield Strength
WDFRX	X-ray Fluorescence with Wave Dispersion

SYMBOLS

ϕ	Diameter (mm)
ω	Rotational speed of the tool (rev/min)
v	Transverse speed of the tool (mm/min)
d_{pass}	Depth of the repeated pass (mm)
n	Number of passes per layer
t	Thickness (mm)

1

INTRODUCTION

1.1 Contextualization

Technological processes for working metals in the solid state have been developed due to the solidification defects commonly found in additive manufacturing processes with aluminum alloys [1]. Several processes within the field of Additive Manufacturing (AM) have been developed for use in the production of metal parts. The urgency for the development of solid-state manufacturing processes has become increasingly necessary, as these processes offer advantages by avoiding the solidification defects visible in other AM processes.

A new process called Friction Rolling Additive Manufacturing (FRAM) appears as a process within this perspective, where through the generation of heat and the addition of continuous material simultaneously, it results in a deposition of the material in layers [2]. Within this process, the use of aluminum as the feeding material allows its handling due to its low melting point and the possibility of, through frictional heating from the tool, making the material visco-plastic and enabling this type of deposition.

After a complete understanding of the process, a method for producing metal matrix composites through the incorporation of ceramic particles will be studied, with the aim of providing other types of characteristics to the part produced. In this context, the application of this FRAM process with materials composed of ceramic particles and the possible advantages and disadvantages of using it will be studied.

1.2 Motivation

The need for optimizing solid-state additive manufacturing (AM) processes is critical for the technological advancement of the industry. Aluminum, due to its low melting point, presents a challenge when used in traditional additive manufacturing processes, particularly because of its tendency to form solidification defects.

This is where Friction Rolling Additive Manufacturing (FRAM) becomes relevant. As an extension of technologies such as Friction Stir Processing (FSP) and Friction Stir Welding (FSW), FRAM offers a solid-state process that relies on the frictional heat generated between a tool and material to create visco-plastic conditions for material deposition.

The proper functioning of the FRAM process required fine-tuning key parameters, because these significantly affect the quality of the produced parts. Additionally, this dissertation investigates the incorporation of ceramic particles within the FRAM process to explore its feasibility as a method for producing metal matrix composites (MMC). The introduction of ceramic particles into the aluminum matrix has the potential to enhance material properties, such as increasing wear resistance, improving the material's ability to withstand high temperatures (thermal resistance), among others.

By contributing to the refinement of the FRAM process and demonstrating the incorporation of ceramic particles, this research aims to advance the capabilities of solid-state AM technologies. It evaluates existing particle incorporation techniques, characterizes the mechanical properties of samples produced with and without ceramic particles, and assesses the effects of varying process parameters on particle distribution and overall material quality.

1.3 Objectives

The main objectives of this work are twofold: first, to thoroughly explore, study, and master the Friction Rolling Additive Manufacturing (FRAM) process as a solid-state metal additive manufacturing (AM) technology; and second, to introduce and investigate the innovative incorporation of ceramic particles within this process. By focusing on the interaction between FRAM and the integration of ceramic particles, especially in aluminum layers, this research seeks to push the boundaries of solid-state AM technology. The work aims to assess the feasibility, challenges, and potential benefits of using ceramic particles to enhance the properties of the deposited metal, ultimately advancing both the understanding and practical application of FRAM. To carry out the FRAM process and the corresponding particle incorporation, several technological objectives were defined, as follows:

- Development of an experimental setup and tools for the operation of the process (design and implementation of a guiding structure for continuous feeding);
- Refine the process parameters;
- Study the feasibility of incorporating ceramic particles through different approaches;
- Characterize the obtained samples using metallographic techniques, uniaxial tensile tests, and hardness tests;
- Characterization of samples taken through visual analysis, micro and macroscopic analysis and mechanical tests;

- Compare the outcome of the samples with particles and without particles, to verify the validation of particle usage in FRAM processes.

1.4 Dissertation´s structure

This document is structured in five chapters.
The state of the art (second chapter) starts by giving an introduction to Additive Manufacturing (AM) in solid-state metals, as well as a review of the existing literature on the FRAM process, which is the subject of this dissertation, covering the various variants that have already been explored. Finally, a literature review is carried out on the incorporation of ceramic particles into metals, the advantages that this process allows, where the main focus will be on the study of their insertion into aluminum.

Chapter 3 presents the description of the materials and equipment planned and obtained for conducting FRAM tests. It began with the presentation of the experimental methodology, followed by the characterization of the materials used in the process. A subchapter followed, focusing on the description of the equipment designed and produced to guide the feeding material during the test, as well as the tool developed and adapted to the parameters used in the tests. It included a subchapter that described all the characterization techniques used on the samples taken from the tests. Finally, it contained a chapter that served as a gateway to the next chapter, consisting of the description of the experimental procedures carried out for each test. Lastly, a brief thermographic analysis of a FRAM test was conducted for the subsequent analysis of thermal values during the test and subsequent discussion of the results.

The following chapter (fourth chapter) presents the experimental results obtained, with the first two subchapters presenting the results and a visual inspection of them for subsequent comparison. It included a subchapter focused solely on the characterization techniques of the samples taken from the tests, where a comparison and discussion of the results obtained were made.

Finally, in the fifth chapter, a survey of the current state is carried out, covering the tasks already completed so far.

2

STATE OF THE ART

2.1 Additive Manufacturing (AM) of metals in the solid state

Additive Manufacturing (AM), also referred to as 3D printing, allows the production of parts layer by layer through the deposition of various materials, potentially without the need for tools [1]. Different types of materials, such as polymers, ceramics, and even metals and metal alloys, have been used in AM, to modify the geometry, dimensions, microstructure and resulting properties [3]. Initially, AM technologies were based on laser beam processes, including Directed Energy Deposition (DED) and Powder Bed Fusion (PBF). Various techniques within this field were developed, leading to 3D printing through the fusion of raw material powders using laser beams. This was followed by the development of electron beam technology, enabling the manufacture of different high melting point metal alloys [1]. The most relevant AM techniques use metal powder or wire as feedstock material, which is melted by a localized heat source and then consolidated, cooled to form a part [4].

However, these techniques are costly due to the need for specialized operators and the possibility of complex post-processing to finish the part. This type of AM also leads to defects such as cracks and porosities, with the main challenge being the use of nonweldable metals in these processes with complex metallurgy such as precipitation-hardening alloys, some tool steels, and cermet's (ceramic + metal) using beam-based AM technologies [1]. Solid-state AM was then developed, divided into two distinct areas: one based on part formation through sintering, transforming powder into parts, and the other based on mechanical deformation of the material to obtain a part [1].
This technique has revolutionized the industrialization of parts through additive manufacturing as it does not require a change in the physical state of a material to obtain another, bringing advantages at the microscopic and mechanical levels. Figure 2.1 shows the classification of different processes within the two aforementioned categories, highlighting the various processes in each category.

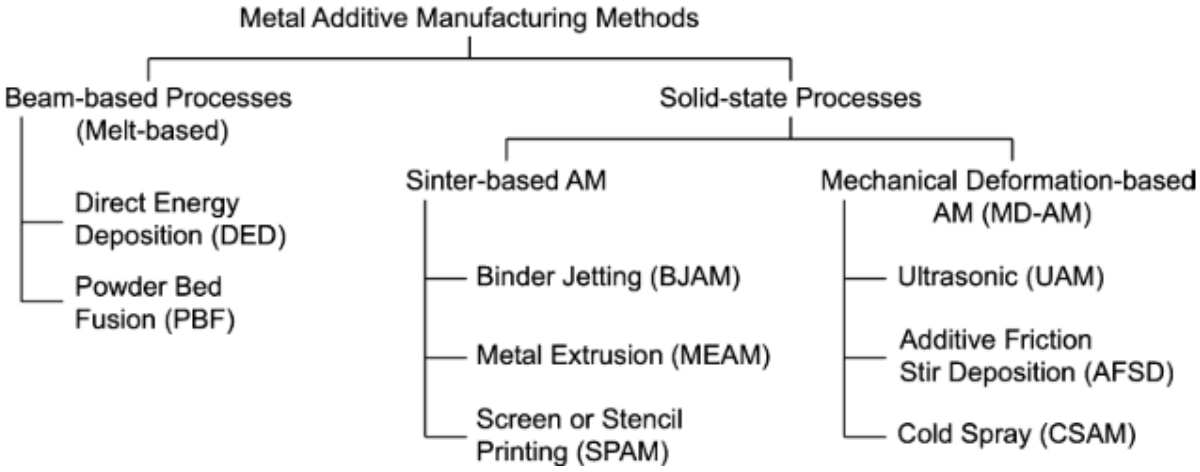

Figure 2.1 - Classification of processes by AM [1].

Within the category of solid-state AM, there is AM based on mechanical deformation, which involves the interaction of oxide layers and subsequent bonding of materials through pronounced plastic deformation. This can be induced by ultrasonic scrubbing, friction, or supersonic impact of powder particles [1]. Among the solid-state AM processes, there are different methods that use solid materials for layer-by-layer production of parts. These methods involve generating heat through contact, such as friction, which makes the material visco-plastic and allows for the deposition and molding of the material onto a base, followed by the overlay of layers to form a part. Compared to casting AM processes, friction-based AM processes generate heat through friction and interlink layers of material through plastic deformation, without requiring full melting of the material for its use in AM [2].

One of the processes used in this context is FSW, an AM process that generates heat through frictional contact between the tool and the material.

It consists of a non-consumable rotating tool that, by heating the material through friction, increases its ductility and joins two pieces or materials through microstructural bonding [5]. This process served as the basis for the development of various solid-state processes, such as Additive Friction Stir Deposition (AFSD). In this process, a feed material, in the form of powder or solid state, is deposited through a hollow shoulder. The rotational movement generates heat through friction, which makes the filler material viscous and causes it to bond to the substrate surface (Figure 2.2) [6].

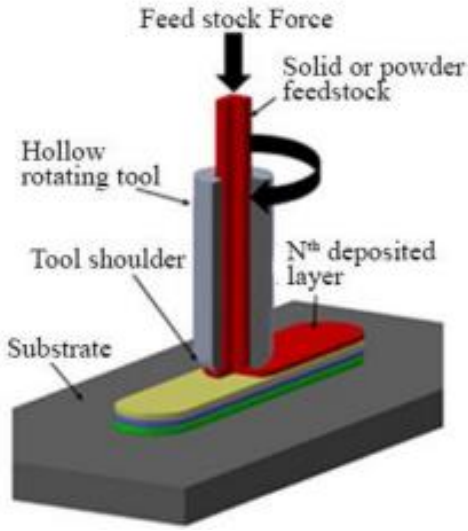

Figure 2.2 - Representative diagram of the AFSD [6].

This process demonstrates the possibility of using powder material for layer-by-layer deposition, aiming to achieve a robust microstructure, similar to FSP and FSW.

With these studied processes, a complementary approach was explored to incorporate particles into a substrate, leading to the production of Metal Matrix Composites (MMC). The literature [7] examined the use of a technological process, Friction Stir Additive Manufacturing (FSAM), for the production of MMC by incorporating copper powder into an aluminum matrix. FSAM involves joining superimposed sheets through a combination of FSW and additive manufacturing processes, as shown in Figure 2.3 a) [8]. Copper powder is placed in the through-holes of the upper sheet (Figure 2.3 b), and with the passage of the rotating tool, the particles are incorporated into the aluminum.

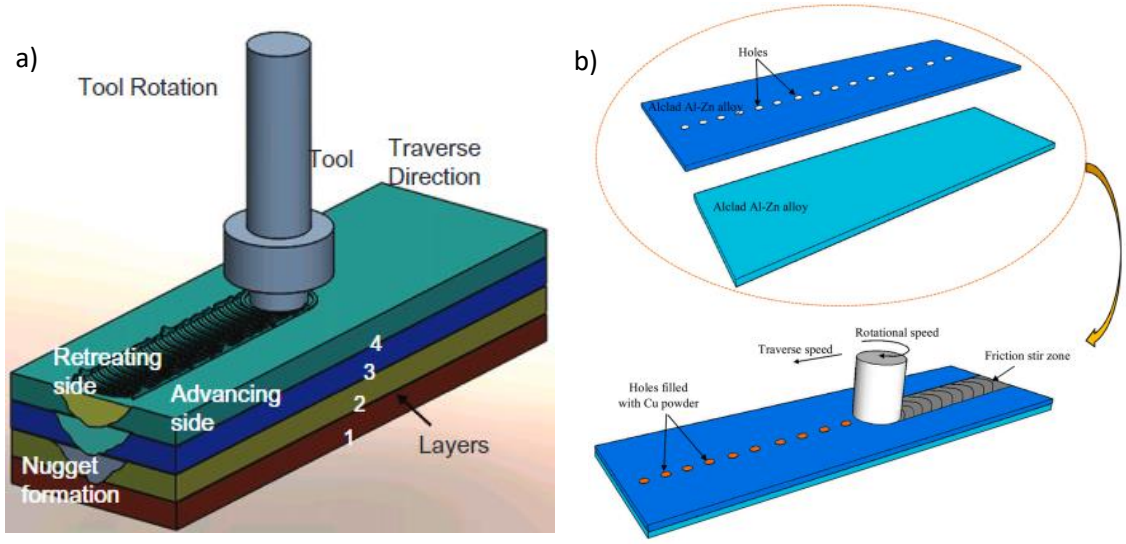

Figure 2.3 - a) Representative diagram of the FSAM process b) Process of MMC production through FSAM [7], [8].

The placement of particles in the substrate and the use of a solid-state process tool have been developed as a technology, as well as the use of grooves in the substrate to accommodate particles and their subsequent incorporation. The key to friction-based additive manufacturing technology is the ability to generate heat in conjunction with continuous material addition [2]. The process to be studied in this dissertation is based on the plastic deformation of metallic materials through heat generation from the friction between the tool, the feeding material, and the substrate, in order to achieve this integration. However, identifying the most viable method for incorporating particles into this process will be the focus of the study, with the aim of determining the best method based on the processes already investigated.

2.2 Fundamentals of Friction Rolling Additive Manufacturing

Friction Rolling Additive Manufacturing (FRAM) is a type of solid-state additive manufacturing for aluminum alloys that revolutionizes the methods of heat generation in the material as well as continuous feeding for deposition [2]. The deposition process is carried out using a horizontal setup, equipped with a rotating, non-consumable tool with a cylindrical head. This process is performed according to the following steps:

1. Before deposition, the tool head starts rotating and is brought into contact with the material (substrate) where the deposition will take place, generating heat through friction between the tool and the substrate (Figure 2.4 a)).
2. Two aluminum wires are continuously used as feeding material at the contact interface and are mixed in the friction zone (Figure 2.4 b)).
3. As the tool tip advances, the feeding wires along with the substrate are deposited along the substrate (Figure 2.4 c)).
4. After completing one layer, the tool is raised to the next layer height and the above process is repeated to build the component (Figure 2.4 d)).

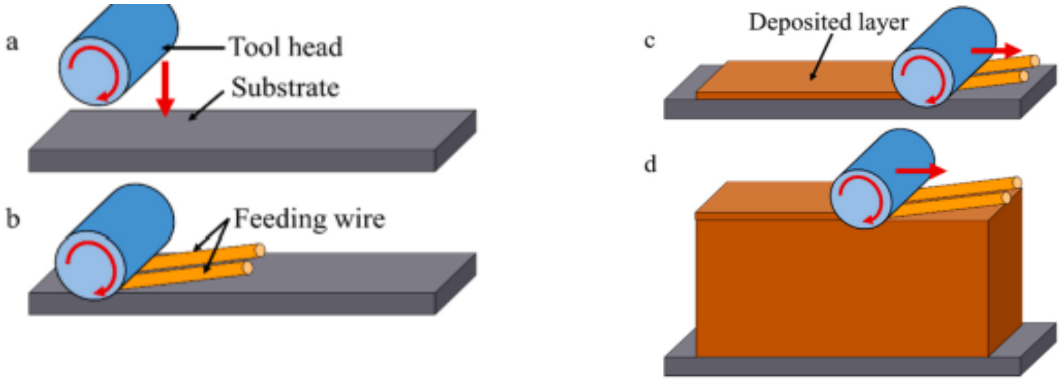

Figure 2.4 - FRAM process diagram of the: (a) head rotation and contact with the substrate; (b) start of wire feeding; (c) deposition through tool advancement; (d) multiple deposited layers [2].

The cylindrical head of the tool was made of tungsten steel, which has excellent hardness and wear resistance at high temperatures. Its dimensions and morphology of the tool head influence the outcome of the process.

A threaded pattern was applied to the surface of the tool to increase the contact area between the tool head and the material, which is beneficial for the heat generation required for the process [2].

As described above, the FRAM process uses aluminum wires as feeding material for creating layers, however it is also possible to perform the process using thinner aluminum strips or metallic powders as feeding materials [9].

2.2.1 Operational parameters of FRAM

One of the major challenges of FRAM is the use of the correct parameters, particularly the tool head diameter (ϕ), the tool rotation speed (ω), the tool transverse speed (υ), and the tool penetration on the substrate (h) [10]. All these factors influence the heat generated in both the substrate and the feeding material, as well as the surface and microstructural qualities of the produced part.

It was concluded in [10] that the rotation speed affects the material flow, as well as the surface finish of the produced part. The higher the rotation speed, the greater the heat generated during material deposition, resulting in a better-deposited surface quality.

Increasing the tool penetration on the substrate affects the amount of material burr, which accumulates on the sides, making the surface more irregular. Figure 2.5 shows a representative image of the process with the mentioned parameters visible.

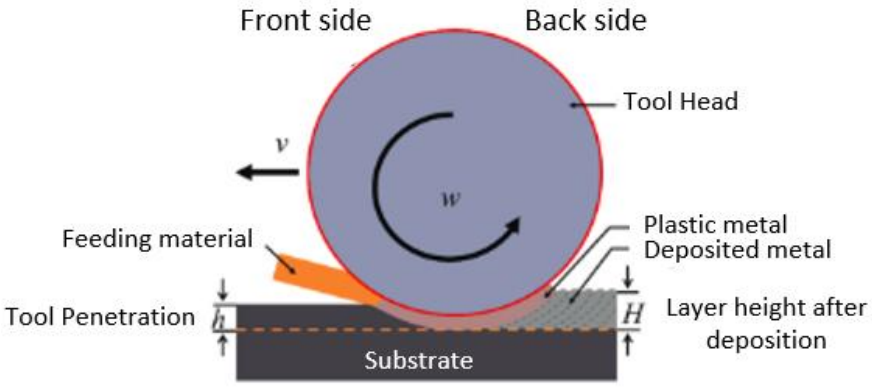

Figure 2.5 - Operational parameters of the FRAM process [2].

Various tests were conducted using tool heads with different diameters, noting the influence of this change on the heat generated by the tool and, consequently, on the material flow in the interaction zone between the substrate, the feeding material, and the tool [11].

2.2.2 Influence of the tool geometry

Different studies on the application of FRAM techniques were analyzed, involving material deposition through non-consumable cylindrical tool tips of varying diameters. This variation impacts various aspects of the process results, such as morphology, deposition rate, material flow, and mechanical properties. In [11], a study was conducted where parts were produced using FRAM with tool heads of different diameters: 25 mm, 50 mm, and 100 mm. Three layers were deposited, each 100 mm in length and 12.5 mm in width. For this study, an Aluminum 6061 T6 plate was used as the feeding material for deposition.

Each tool head is made of H13 steel, and its geometry is shown in Figure 2.6.

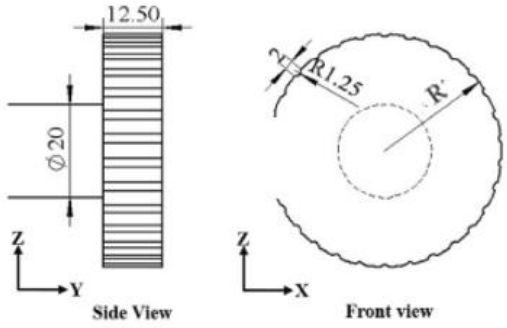

Figure 2.6 - Geometry of the tool head used [11].

In the conducted tests, the characteristics adopted are outlined in Table 2.1, along with the nomenclature used for each sample taken.

After the conducted tests, an analysis of the morphological surface of the results was performed. This visual analysis of the samples, shown in Figure 2.7, allows for an assessment of their surface quality. With the 25 mm diameter tool (Figure 2.7 a)), a constant fish-scale pattern is observed. Increasing the rotation speed intensifies this pattern, resulting in worse surface finishes. With the 50 mm diameter tool (Figure 2.7 b)), the morphology displays a larger fish-scale pattern, which tends to increase with higher rotation speeds, resulting in rougher and less desirable finishes. Using the 100 mm diameter tool (Figure 2.7 c)) with transverse speeds below 260 mm/min results in surface finishes with higher roughness.

Table 2.1 - Experimental parameters of FRAM tools with different diameters adapted from [11].

Toolheads diameter (mm)	Sample name	Tool height (mm)	Transverse speed (mm/min)	Rotation speed (rev/min)
25	A1	0.8	80	800
	A2		100	800
	A3		80	1000
	A4		100	1000
50	B1	0.8	80	800
	B2		100	800
	B3		80	1000
	B4		100	1000
100	C1	0.8	100	800
	C2		150	800
	C3		150	1000
	C4		200	1000
	C5		260	1000
	C6		300	1000

.

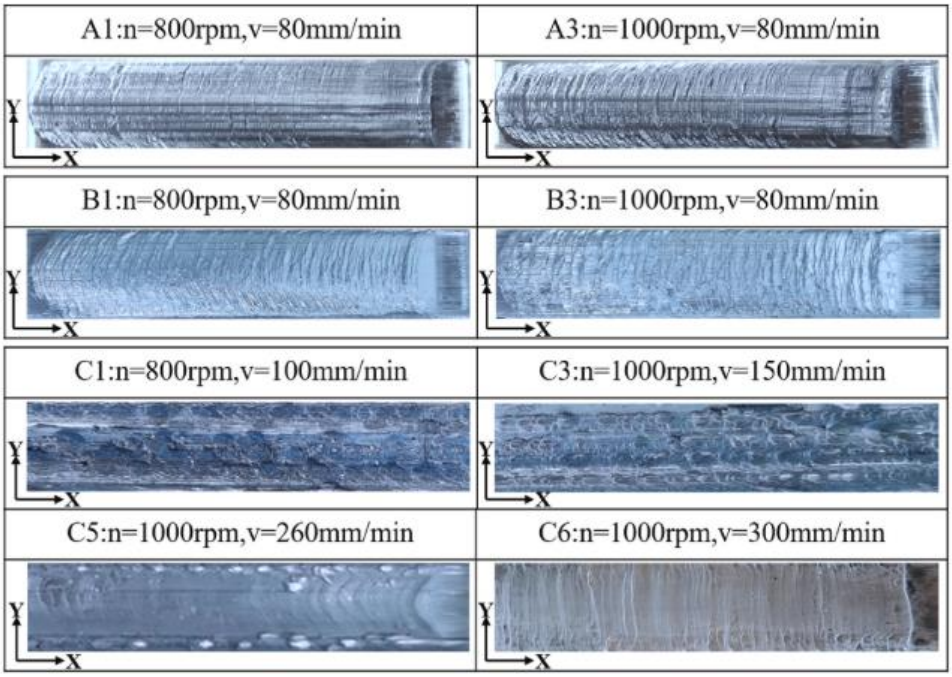

Figure 2.7 - Surface morphology of samples with tool diameters of: a) 25mm; b) 50mm; c) 100mm [11].

Liu et al. [11] concluded that the effect of temperature in the interaction zone (the area between the feeding material, the substrate, and the tool) is highly relevant to the results obtained, as it affects the degree of plastic deformation of the feeding material, as well as the material flow, also influencing the morphological characteristics of the deposited material, the quality of the layer bonding, and the associated mechanical properties.

The maximum temperature reached during the FRAM process is directly proportional to the diameter of the tool tip for the same process parameters. In other words, the temperature relationship with respect to the diameters is:

$$T_{Toolhead\ diameter\ 100\ mm} > T_{Toolhead\ diameter\ 50\ mm} > T_{Toolhead\ diameter\ 25\ mm}$$

This is due to the fact that the larger the tool diameter, the greater the linear speed, which consequently generates more heat in the friction zone, leading to an increase in the tool temperature. The temperatures recorded during the process ranged from 71.1% to 96.2% of the melting temperature of the aluminum strip used.

It was also concluded that when a larger toolhead diameter is used, the method to make the plate in the interaction zone more viscous is to increase the transverse speed, as it reduces the maximum temperature reached, shortens the time to reach the material's melting point, and improves its flow.

Increasing the transverse speed of the tool enhances the efficiency of the FRAM deposition process. The tool diameter also affects the heat production in the interaction zone between the tool, the substrate, and the feeding material. This diameter directly influences the tool's contact area; a larger radius increases the contact area, which in turn increases the thermal input to the process.

It was also noted that the contact between the toolhead and the substrate or layer during material deposition affects the results, potentially altering the material's viscosity and deposition efficiency. Several tests were conducted with different penetrations on the substrate. Figure 2.8 shows Optical Microscopy (OM) images of each test, with the arc representing the migration zone of the material from the plate in the interaction area marked in yellow [11].

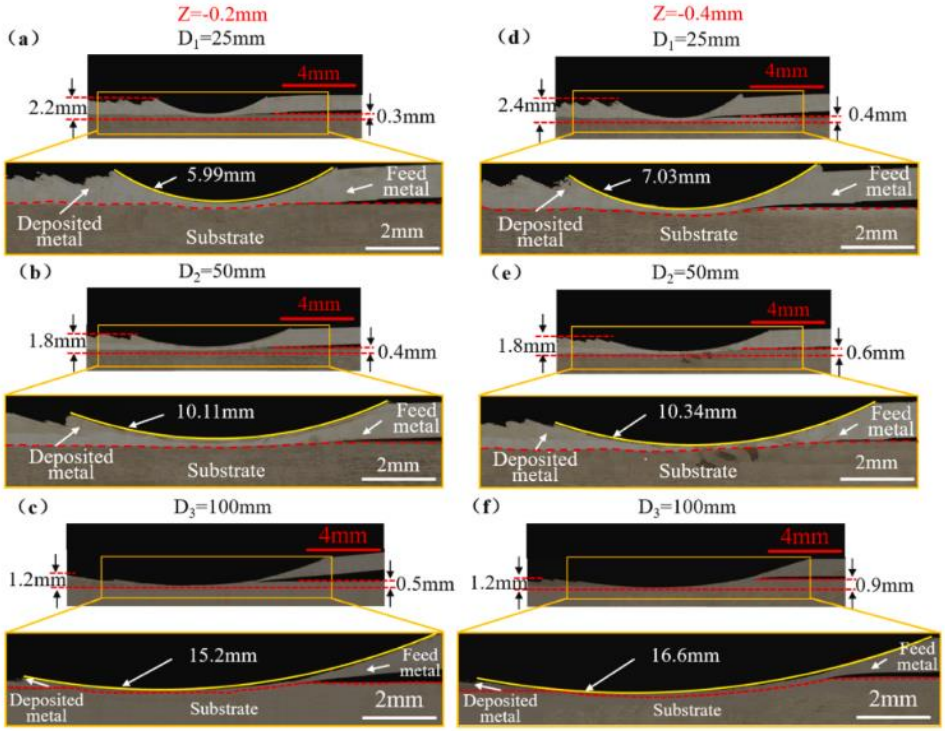

Figure 2.8 - OM results for different diameters with different depths, being: a) 25 mm, b) 50 mm and c) 100mm with a depth of 0.2mm; d) 25mm, e) 50mm, and f) 100mm with a depth of 0.4mm [11].

It was concluded that with the increase in the diameter of the toolheads, the arc of the interaction zone also increases, resulting in a higher heat input per unit time, which affects the patterns of plastic deformation [11].

With larger diameters, plastic deformation becomes more intense, leading to a decrease in the material's viscosity and transfer efficiency. Consequently, a layer of material accumulates on the surface of the toolhead, altering the distance between it and the substrate.

It was also observed that the viscosity coefficient $(1 - \delta)$ of the plate decreases as the diameter of the tool used increases, as shown in Figure 2.9. This is due to the fact that when the toolhead diameter increases, there is a greater thermal input into the feeding material, weakening the plastic flow behavior in the interaction zone and leaving it in a more liquid state.

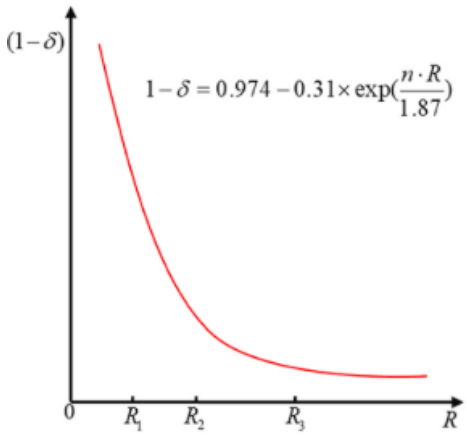

Figure 2.9 - Schematic diagram of the material viscosity variation related to the variation in tool head diameter [11].

The conclusion drawn from the analysis of each aspect underlines the importance of carefully selecting the parameters of the FRAM process to ensure the desired quality and performance of the materials deposited.

2.2.3 Microscopic analysis, mechanical testing and material flow

Xie et al. [2] conducted a test using a horizontal CNC machine (Figure 2.10), where the feeding material consists of two ER6061 aluminum wires and the substrate is an Aluminum 6061 alloy plate. The tool used has a non-consumable head with an outer diameter of 20 mm and a threaded surface to facilitate material flow. In [1], it was concluded that using threaded surfaces on the tool tip promotes improved material flow in the plastic regime, which is beneficial for mixing layers at the deposition interface.

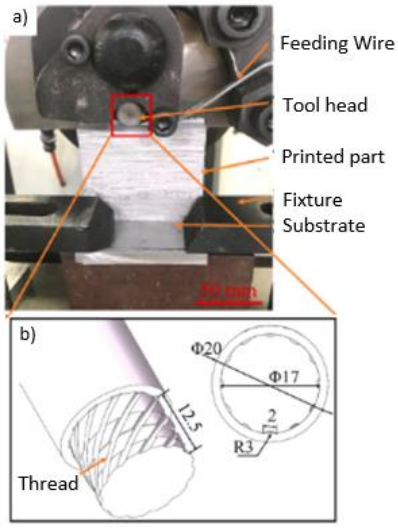

Figure 2.10 - FRAM process equipment: a) in operation b) tool head [2].

Through Figure 2.11 a), it was concluded from optical microscopy (OM) analysis that it is possible to achieve a dense microstructure with minimal defects. The layers achieved bonding without melting of the material, reaching 60-90% of its melting temperature. Before magnification of the analyzed sample, the boundaries between layers are invisible (Figure 2.11 b). When magnified, these boundaries become visible and show no defects, such as porosities or oxide layers (Figure 2.11 c). The reason that adjacent layers can form a bond without melting is that the rotating tool is pressed onto the surface of the current layer, meaning that the material of the current layer undergoes secondary friction, allowing it to blend with the adjacent layer (feeding wire), which provides a metallurgical bond.

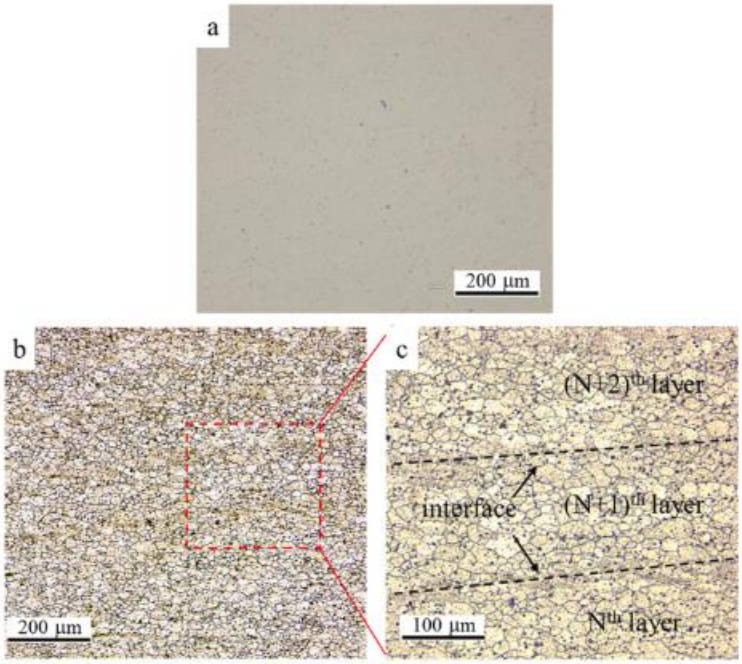

Figure 2.11 - OM images of the sample: a) before magnification, b) after magnification with focus on an area in c) [2].

The first plasticized material formed contains fine and elongated grains, while its interior has equiaxed and refined grains. This is due to the pronounced plastic deformation on both sides of the boundaries with the adjacent layer [12].

Xie et al. [13] obtained a similar structure using two ER2319 aluminum alloy wires as the feeding material. A stable bonding between layers was achieved, visible at the microscopic level, with a focus on the analyzed area where no defects, such as pores or cracks, were detected.

Xie et al. [10] also conducted a test using a plate as the feeding material. The microscopic result was similar, showing equiaxed grains in the adjacent layer (12.5 µm), while the previously deposited layer had even more refined grains (3.5 µm).

An additional test was performed with the feeding material in contact with the substrate, concluding that the grain size after the FRAM process became more refined, changing from elongated to equiaxed.

A strong bond between the two layers was noted, dense and free of porosities or defects associated with this bonding [14].

Xie et al. [2], using Electron Backscatter Diffraction (EBSD) for material characterization, concluded that the grain size of the deposited material is reduced compared to the feeding material due to dynamic recrystallization caused by the pronounced plastic deformation (Figure 2.12 a) and b)). Figure 2.12 c) and d) show that the grain size in the YZ plane is smaller than in the XZ and YX planes because the area of plastic deformation in the YZ plane is greater than in the other planes.

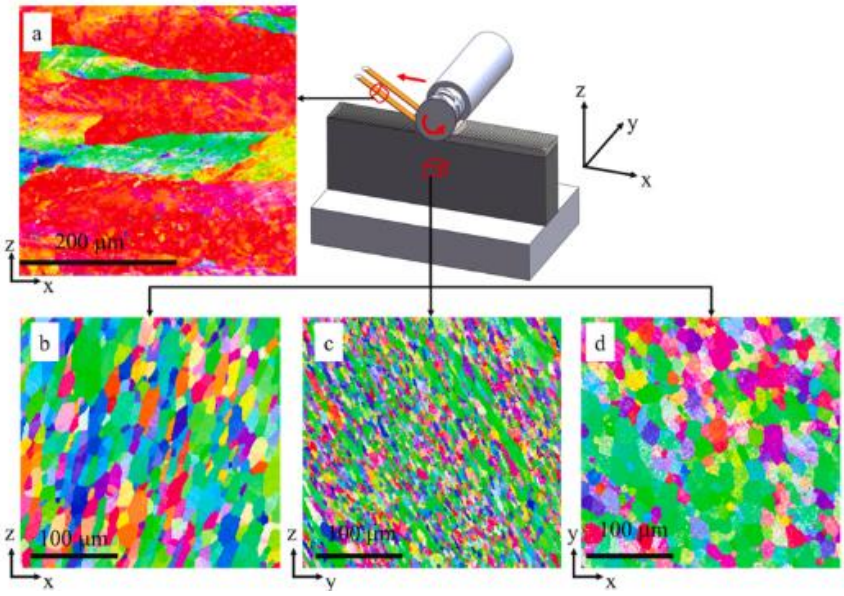

Figure 2.12 - EBSD Map of a) feed wire and deposited material in b) XZ Plane, c) YZ Plane, and d) XY Plane [2].

Uniaxial Tensile tests were conducted to observe the mechanical properties of the produced part. Three specimens were taken horizontally from different positions and three vertically from different positions of the final part (Figure 2.13 a), and were subjected to the test, with the results presented in Figure 2.13 b). These tests were used to study the Yield Strength (YS), Ultimate Tensile Strength (UTS), and elongation [2].

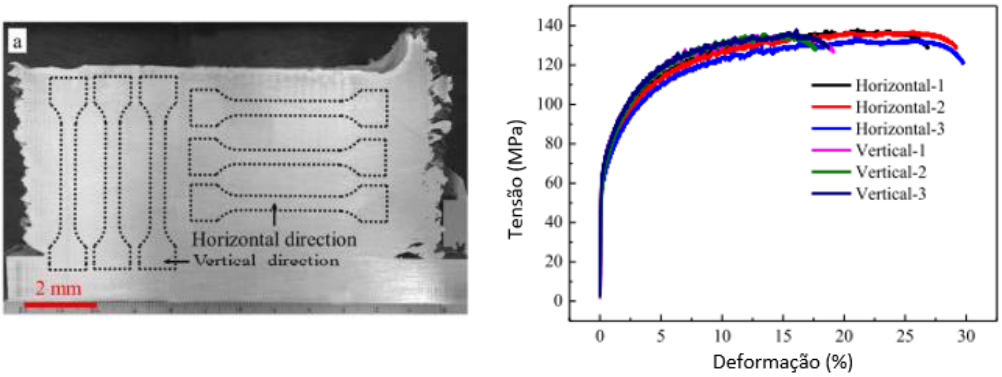

Figure 2.13 - Tests conducted on the final piece with a) different types of specimens and b) their ETU results [2].

It was concluded that the UTS and YS in the horizontal direction are slightly higher than in the vertical direction. However, the elongation in the horizontal direction is significantly greater than in the vertical specimens, as the grain size in the YZ plane is smaller than in the XZ plane.
In articles [2] and [3], analyses were performed using Scanning Electron Microscopy (SEM) on the fracture surfaces of the specimens, where it was observed that the fracture morphology indicates ductile fractures, confirming extensive elongation in both horizontal and vertical specimens. The number of cavities in the horizontal direction is greater than in the vertical direction, which confirms the superior elongation in the horizontal direction. Figure 2.14 shows the results of this analysis from article [2].

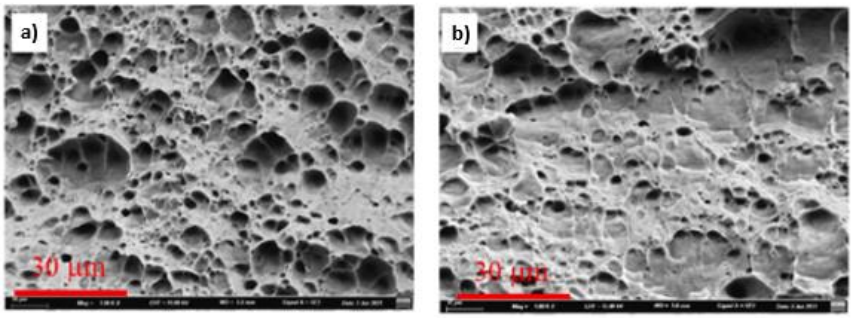

Figure 2.14 - SEM analysis results of the fracture surface of the sample a) horizontal b) vertical [2].

Despite the promising results of this process, the technique still requires refinement in both the parameters and the equipment used. However, with the current equipment, it was possible to produce parts for studying them with the aim of improving these aspects.

2.3 Applicability of the FRAM process

Although the process is still the subject of many studies and adaptations, FRAM is already included in repair processes, such as removing material from a zone or even adding material to a specific zone. Liu et al. [14] tested the repair of grooves (rectangular or trapezoidal fabricated cavities) using the FRAM process. This involves the deposition of material, just like the usual FRAM process, but this time the deposition is carried out in the grooves. The main challenge was the need to adjust the height of the toolhead relative to the substrate, which is a key factor for the complete filling of the cavities. In Figure 2.15 a), the sequence of processes performed in this study is shown, and in Figure 2.15 b), the equipment setup during the process is visible.

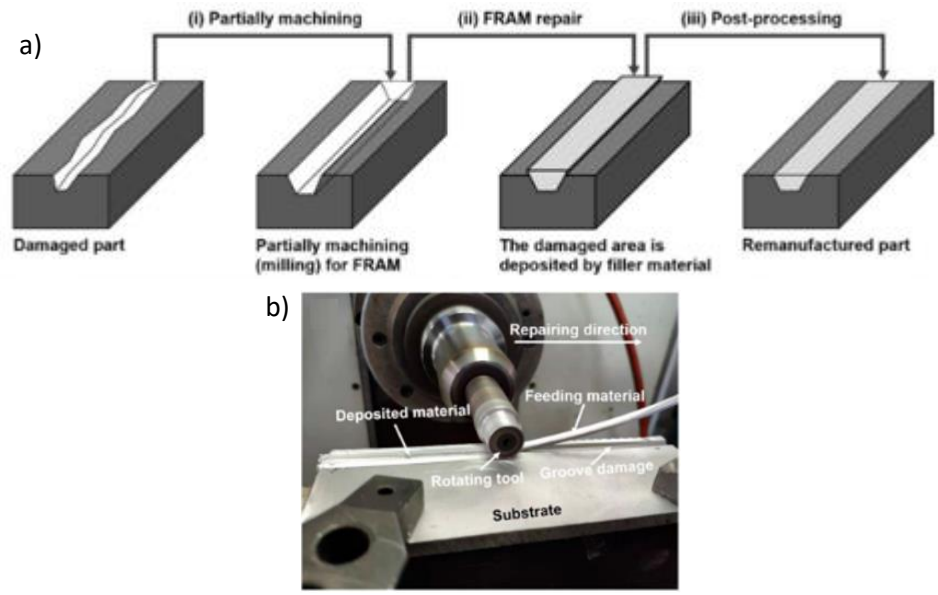

Figure 2.15 - Schematic diagram of the repair process: a) defect surface repair using machining and FRAM b) FRAM repair process [14].

In this process, a modified horizontal CNC machine was used, where both the substrate material and the feeding material are 6061 Aluminum Alloy. In this study, the reliability of the FRAM process in repairing grooves was explored through the repair of three types of grooves (rectangular, trapezoidal, and V-shaped), with the following process parameters: tool rotation speed (n = 1000 rev/min); transverse speed (v = 60 mm/min); tool penetration on the substrate (h = 1.70 mm). To investigate the influence of the tool penetration in this process, other tests were conducted where the penetration was 1.50 mm and 2 mm.

It was concluded that a successfully repaired joint was obtained when the tool penetration was 2mm. Microscopic analysis revealed a complete connection between the substrate and the feeding material [14]. In Figure 2.16, we can see a microscopic comparison of the interface between the feeding material and the substrate for each test. Figure 2.16 c) clearly shows the complete union between them.

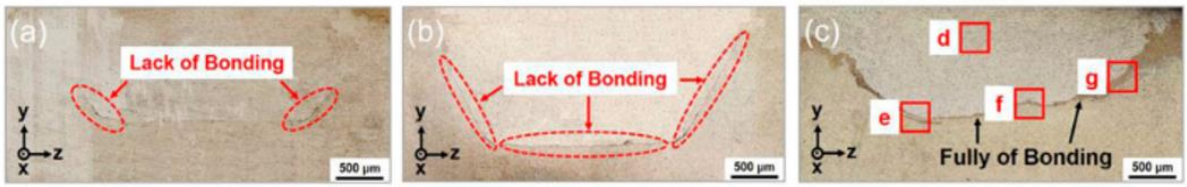

Figure 2.16 - MO results of the trapezoidal groove repair with deposition height of: a) 1.70 mm; b) 1.50 mm; c) 2 mm [14].

It was also concluded that equiaxed grains formed in the repair area, and refined equiaxed grains formed in the refinement zone, which is the interface between the substrate and the repair area, as seen in Figure 2.17. This process proved promising for the repair of such defects, with particular attention given to adapting the tool height parameter to the substrate for a better bond between the substrate and the deposited material.

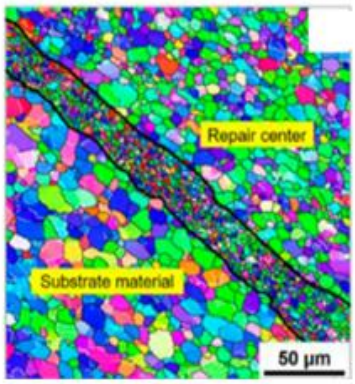

Figure 2.17 - Grain morphology at the interface of the repaired joint [14].

2.4 Ceramic particles in metallic materials

Metal Matrix Composites (MMC) are materials used in modern industry with the goal of providing new characteristics to a base metal matrix. The main objectives for the development of MMCs include increasing strength, creep resistance, fatigue strength, thermal shock resistance, corrosion resistance, Young's modulus, and reducing thermal elongation [15]. MMCs can be classified based on the type and contribution of the reinforcing components [15]. In Figure 2.18, the existing classification of an MMC is represented.

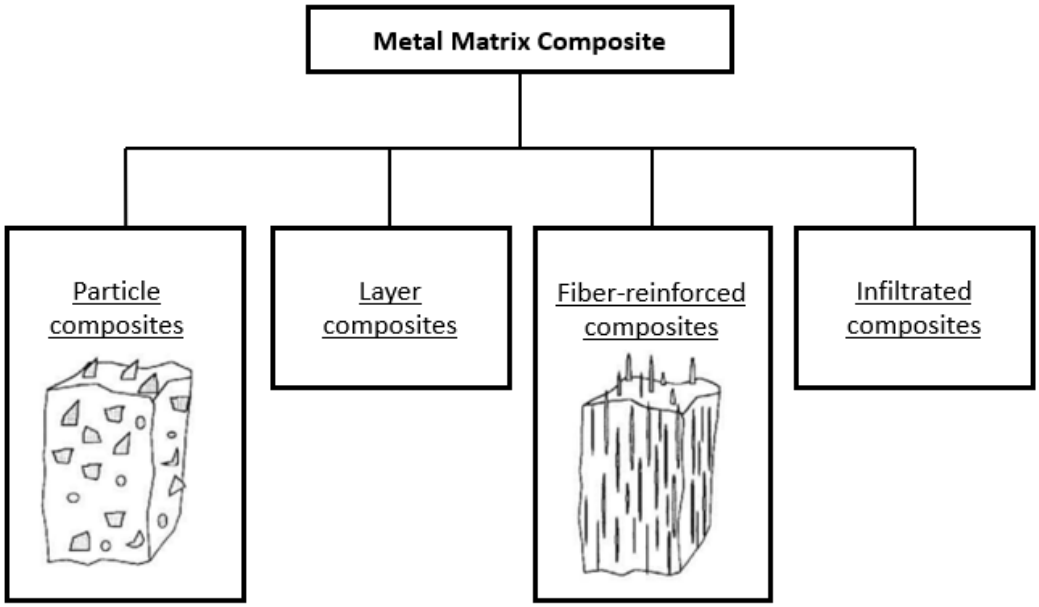

Figure 2.18 - Classification and schematic representation of different types of CMM adapted from [15].

The incorporation of ceramic particles into metallic matrices has emerged as a promising technique for improving the mechanical properties of metallic materials [16].
Due to various properties such as good strength-to-weight ratio, high thermal conductivity and good corrosion resistance, aluminum alloys have become very popular as structural materials; however, their applications have been limited due to their relatively low wear resistance.

The use of ceramic particles, such as silicon carbide (SiC) and aluminum oxide (Al_2O_3), as reinforcing agents in the formation of aluminum matrix composites has been well studied. Recent studies have shown that for a fixed concentration, inclusions of small particles usually produce stronger composites with a higher hardness [17].

2.4.1 FSP with ceramic particles

The FSP has been shown to be effective in incorporating ceramic particles into solid state materials. It has emerged as a highly effective solid metal handling technique in the production of aluminum matrix composites, with the aim of improving the hardness of the substrate material and its resistance to wear while maintaining its ductility and conductivity [16]. Figure 2.19 shows the FSP used to insert and mix ceramic particles into an aluminum substrate.

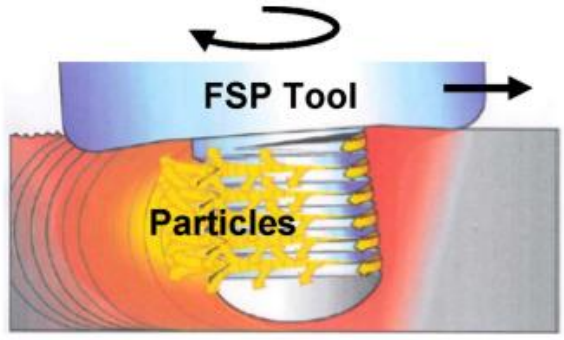

Figure 2.19 - FSP in particle insertion into aluminum [16].

In the study conducted by Dinaharan [18], the aluminum alloy AA6082 was chosen as the matrix material, and various ceramic particles, including SiC, Al_2O_3, titanium carbide (TiC), boron carbide (B_4C), and tungsten carbide (WC), were used as reinforcements. FSP facilitated the homogeneous surface dispersion of the ceramic particles throughout the material mixing zone. The resulting debris blended perfectly with the aluminum in its plastic state, contributing to a well-dispersed and uniform microstructure.

Dinaharan [18] highlighted the strong bond between the aluminum matrix and the ceramic particles. Additionally, mechanical properties such as hardness and UTS were significantly improved in all aluminum alloys compared to the base aluminum alloy. The effectiveness of FSP in adapting the microstructure and mechanical performance of the alloys was also emphasized.

It was incorporated SiC reinforcement particles, a material with high hardness, using a variant of FSP called Upward Friction Stir Processing (UFSP), which innovated CMM production capacity by dispersing functional particles in a metal matrix with an upward flow. The particles are completely dispersed throughout the machined volume. However, the distribution is not completely uniform compared to the FSP test [19]. Figure 2.20 shows a schematic representation of the process described.

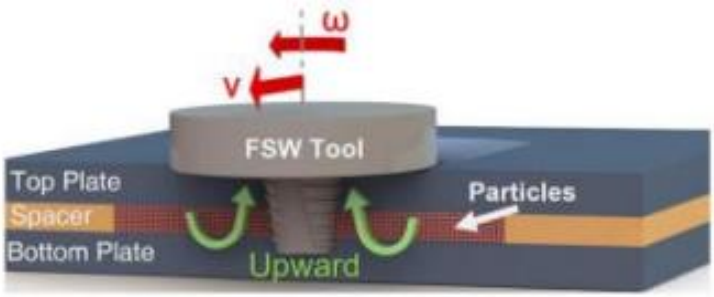

Figure 2.20 - Schematic representation of the UFSP process [19].

Silicon carbide (SiC) particles were incorporated between two plates of 7075-T651 aluminum alloy using a spacer to prevent the dispersion of the particles. When used as a reinforcing material, SiC particles increase the hardness of the matrix, enabling changes in the material's properties that were previously solely metallic.

In addition to this process, extrusion and rolling are also commonly used methods for incorporating ceramic particles into metal matrix materials. Each of these methods has its drawbacks concerning the morphology achieved after particle incorporation. Consequently, different processes are used based on user preference for each specific application. Most processes tend to produce surface-layered MMC, while those aiming for distribution throughout the volume often result in a homogeneous but non-uniform distribution of particles [16].

2.4.2 Sensorial Particles

Rather than blending particles into molten material, solid-state processing through Friction Stir Processing (FSP) can be used to introduce and distribute particles in metallic components via visco-plastic stirring phenomena [20]. Incorporating sensor capabilities into metallic components has been a longstanding challenge in materials engineering, often made more complex by the difficulties of integrating external sensors [21]. The addition of sensor particles in metal matrices has been frequently tested in solid-state additive manufacturing processes. Their incorporation into the FRAM process could prove to be interesting, as it is a process similar to FSP.

The inclusion of piezoelectric materials into metal matrices by FSP has shown to improve the mechanical and/or to modify electrical properties of the base material [20]. Consequently, piezoelectric materials represent an opportunity for the development of self-monitored materials. Figure 2.21 represents the schematics of the production of a self-sensing material.

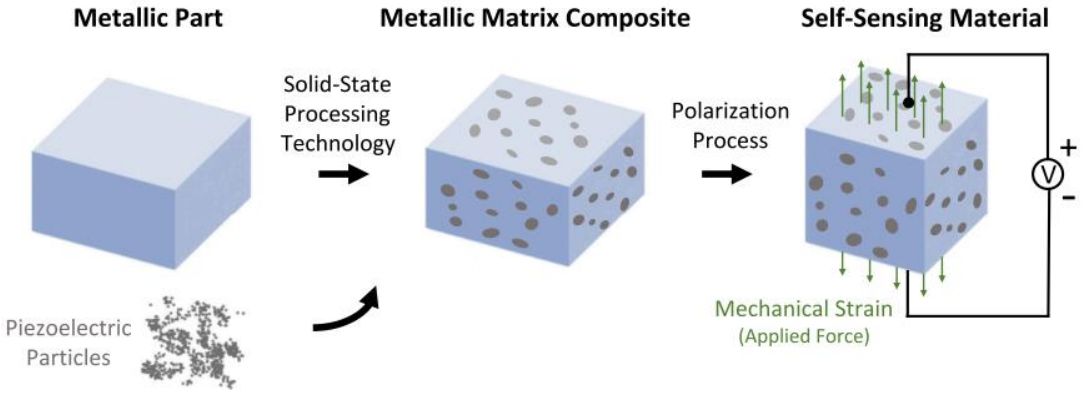

Figure 2.21 - Schematic representation of the self-sensing material development steps [20].

The production of self-sensing materials brings multiple advantages to the AM industry. By utilizing stimulus-responsive properties, such as electrical conductivity, self-sensing materials can detect and report on various stimuli, including mechanical deformation, pressure, moisture content/humidity, pH, temperature and others [22]. One of the key advantages of piezoelectric-based materials lies in their ability to provide spatially continuous sensing [23]. Studies conducted at [24] demonstrated a 22%-30% increase in the maximum processing temperatures reached during the process due to the presence of piezoelectric particles. In addition to an improvement in the processed zone, these materials showed remarkable potential for detecting changes in stress and evaluating structural integrity [21]. The insertion of particles in solid-state additive manufacturing processes has proven to be advantageous for the development of metallic material properties. Implementing this knowledge in the FRAM process is something to explore, and it may offer similar advantages.

3

MATERIALS AND METHODS

In this chapter, the methodology to be followed for the study of the FRAM process with metallic materials incorporated with ceramic particles was presented in order to meet the previously established objectives.

3.1 Characterization of substrate and feeding material

For the experimental analysis and subsequent testing, this dissertation utilized different types of aluminum for both the addition material and the substrate in the production of walls via FRAM.
For the substrate, AW5083 aluminum plates were used, with a thickness of 10 mm and dimensions of approximately 90x40 mm in length and width. The chemical composition of these plates is presented in table 3.1, according to the technical data provided by the manufacturer (PolyLanema) and the MATWEB website. This material was chosen for the substrate due to its good heat conductivity, which is crucial for material deformation during testing, as well as its ease of welding, since it is preferable to use a substrate that quickly heats up and cools down.

Table 3.1 - Chemical composition of the 5083-H112 aluminum alloy.

Elements	Al	Cr	Cu	Fe	Mg	Mn	Si	Zn	Ti
[%]	92,4 – 95,6	0,05 – 0,25	≤ 0,1	≤ 0,4	4,0 – 4,9	0,4 - 1	≤ 0,4	≤ 0,15	≤ 0,25

For the feeding material, 2 mm thick aluminum strips were used, measuring approximately 10 mm in width and 90 mm in length. These strips were cut according to the length of the deposition area on the substrate.

The characterization of this material was carried out using three samples of the addition material. X-ray Fluorescence with Wave Dispersion (WDFRX) tests were performed with the X-ray Zetium WDXRF Spectrometer from Malvern Panalytical.

The main objective of this analysis was to determine the chemical composition of the addition material used. After comparing the results from the three samples, it was concluded that there is no discrepancy between them. Therefore, we are indeed dealing with an AA1040 aluminum alloy with the chemical composition represented in Table 3.2.

Table 3.2 - Chemical composition of the feeding material tested.

Elementos	Al	Fe	Si	Zn
[%]	99,4	0,141	0,416	0,0223

Table 3.3 below presents the physical and mechanical properties of the two types of aluminum used in this study.

Table 3.3 - Mechanical properties of the 5083-H112 aluminum alloy and the 1040 Aluminum Alloy.

Mechanical properties	**Aluminum Alloy 5083 - H112**	**Aluminum Alloy 1040**
Yield Strength	190 MPa	195 MPa
Ultimate Tensile Strength	300 MPa	238,6 MPa
Poisson coefficient	0,33	0,33
Young´s modulus	70,3 GPa	69 MPa
Thermal conductivity	117 W/mK	117 W/mK
Melting point	590,6 – 638 ºC	500 – 600 ºC
Density	2660 kg/m^3	2705 kg/m^3

3.2 Characterization of Ceramic Particles

During the experiments of this process, the feasibility of incorporating ceramic particles into walls fabricated by FRAM was studied. For this study, Silicon Carbide (SiC) particles were used to subsequently form MMC. MMC incorporating SiC particles into an aluminum matrix are promising for aerospace, automotive, military, and sports industries.

Compared to the substrate (aluminum alloy) into which they are incorporated, SiC particles tend to have higher fatigue resistance, higher Young's modulus, and greater hardness, characteristics that offer clear advantages in mechanical properties, making them suitable for various applications in these sectors [25]. The FRAM manufacturing process introduced SiC ceramic particles with a purity of 99.5% and a particle size of 35 μm.

During the different experiments, various methods for incorporating the particles were tested, with the main priorities being:

- Ensuring homogeneous dispersion of the particles throughout the section;
- Ensuring mixing of the particles with the substrate;
- Ensuring dispersion of the particles in the largest possible volume of the part.

3.3 Experimental Setup for FRAM

3.3.1 Equipment used in FRAM

For conducting the FRAM tests, a three-axis conventional milling machine (Figure 3.1) was used. This machine allows for precise control of process parameters, including transversal speed, rotational speed, and tool penetration on the substrate. The equipment is located in the Mechanical Processes Laboratory of the Department of Mechanical and Industrial Engineering at the NOVA School of Science and Technology.

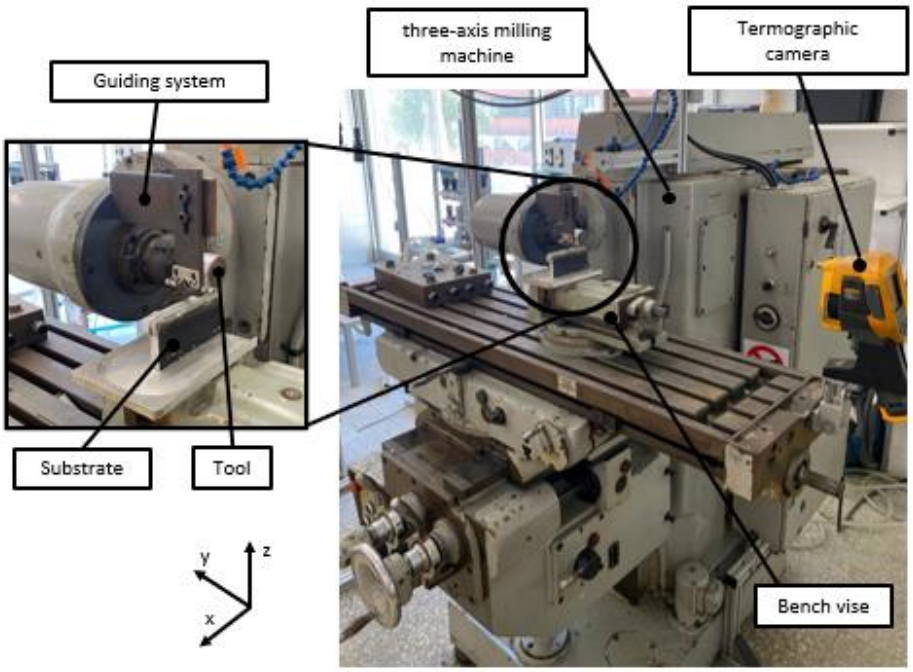

Figure 3.1 – Experimental setup for the fabrication of walls by the FRAM process and identification of each element used during the operation of the process.

This equipment is well-suited for the tests as it is derived from the FSP manufacturing process and, with the appropriate modifications, the forces involved are similar to those required for the FRAM process. During the operation of this process, it was necessary to control the three aforementioned parameters through different zones of the machine, which are, rotational speed, transversal speed, and tool penetration on the substrate.

To adapt this equipment for the FRAM process, the tool head was tilted at 90º to facilitate the deposition of the feeding material during the process, as well as to secure the substrate to the milling machine table. Both the position used during the process and the three parameters controlled are depicted in Figure 3.2.

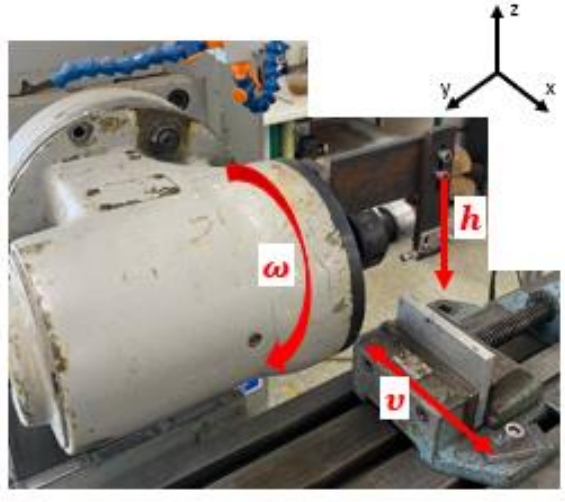

Figure 3.2 - Milling machine head tilted along with the three process parameters.

3.3.2 Guiding system of the feeding material

The guiding system designed and implemented for the FRAM process is shown in Figure 3.3. Its main objective is to enable continuous and stabilized feeding of the material added. The geometry of the system was designed to allow horizontal feeding of the material to the deposition zone on the substrate and to secure the feeding material without impeding its movement during the process. This clamp can be divided into two individual parts: the horizontal arm relative to the milling machine and the vertical arm, which will contact the feeding material.

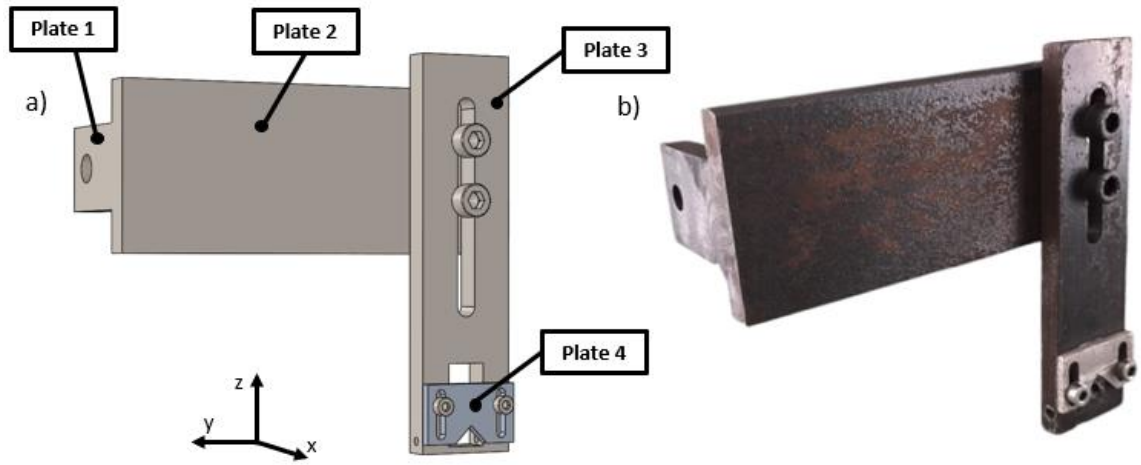

Figure 3.3 - Guiding system for conducting FRAM tests: a) 3D CAD model; b) manufactured component.

Starting with Plate 1, with 8 mm thick, cut to the dimensions described in Figure A.1. The Plate 2, with the same thickness, is placed against the milling machine, designed to connect the system to the machine through a hole with a diameter of 6.5 mm. Plate 2, positioned horizontally and serving as the connection to the vertical arm, is welded perpendicularly on the smaller plate to ensure a solid connection.

Plate 2 has two vertical holes, equally spaced from its edges, with a diameter of 6 mm, allowing connection with the vertical arm and providing horizontal constraint while enabling free vertical movement. This allows for adjustments in the distance between the feeding material, the tool, and the substrate.

Regarding Plate 3, all dimensions are represented in Figure A.2 and it is designed with the following characteristics:

- A steel plate, long enough to reach the deposition area of the feeding material on the substrate, with a through slot to allow vertical movement. At the other end, a rectangular slot, parallel to the edges of the plate, was made to accommodate the feeding material.
- An aluminum plate (Plate 4) with vertical slots at the top and bottom, to ensure the vertical constraint of the feeding material (technical drawing shown in Figure A.3).
- Two through holes above and below the rectangular slot, to accommodate the bolted connection of the aluminum plate.
- Threaded holes made at the top and bottom of the steel plate, in the area where the feeding material will pass through. With the help of a screw in each hole, a top and bottom tightening was made to ensure the horizontal constraint of the feeding material, as well as the centralization of the feeding material with the substrate. The use of two nuts on each screw ensures their tightness on the feeding material.

Regarding the manufacturing processes used to produce the guiding system, a piece of steel with dimensions 260 × 60 × 8 mm was used. Using a band saw, the steel was cut into three individual plates. On Table B.1 is a table that describes the processes used to create the necessary geometries for each plate.

After conducting the tests, it was noted that the area designed to prevent the vertical and horizontal movement of the feeding material, as initially defined, was insufficient. When changing the profile used during the process, the methods for securing it also changed, which was not practical.
To address this issue, the aluminum plate was adapted by making a triangular cut in the area where the feeding material rests. This modification aimed to prevent both vertical and horizontal movement while allowing the use of different profiles without stopping the process. Figure 3.4 shows the aluminum plate with the triangular cut.

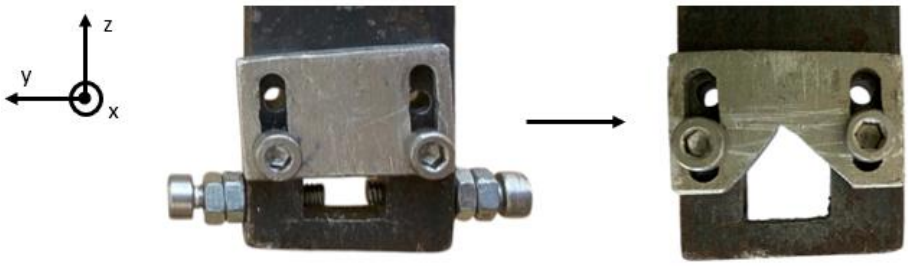

Figure 3.4 - Evolution from the initial version to the final version of the machined aluminum plate for the guiding system.

3.3.3 Development of the tool in the process

For the successful execution of the FRAM process, it was essential to plan the geometry of the tool to be used. Initially, the process was tested with the tool shown in Figure 3.5 a), but it was observed that the contact area between the tool and the substrate, as well as the feeding material, was insufficient relative to the geometry of the other two elements. Consequently, a new tool was produced from Hardened Steel CK45, which increased the contact area both transversely and in diameter.
The tool consists of the main body, which features a larger diameter working area with a patterned surface designed to enhance the deposition and friction of the feeding material on both the substrate and the tool, referred to as the tool head. The tool's characteristics, along with all its dimensions, are detailed in Figure A.4. To ensure the tool's durability, it was flame-hardened to increase its resistance to fatigue, as the process heavily depends on the friction generated. Figure 3.5 b) shows the tool after it has been flame-hardened.

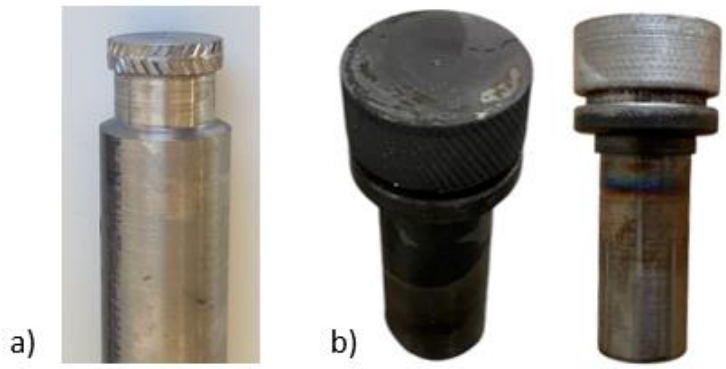

Figure 3.5 - Tool used for FRAM tests: a) pre-optimized;
b) post-optimized and flame-hardened.

3.4 Experimental procedure

This chapter describes the entire experimental procedure carried out in the various FRAM tests, including preparatory work and experimental setup for each test.

The process began with preliminary FRAM tests aimed at studying the operation of the process, the technique adopted for using the feeding material, and the positioning of the substrate. Next, attention was directed towards conducting tests on larger walls, followed by sampling and characterizing them using different techniques. Finally, with standardized parameters and established procedures, walls with ceramic particle incorporation were produced, and samples were extracted and analyzed.

In addition to the FRAM tests, with and without ceramic particles, a significant part of the experimental procedure involved problem-solving and overcoming obstacles inherent to the process, given its relatively unstudied nature, as well as the preparatory and setup phases required for its execution.

3.4.1 FRAM Tests

To begin the FRAM tests, the experimental setup for the process was first assembled. To ensure that the substrate is positioned correctly, a standard block is placed underneath it when mounted on the bench vise, achieving a height that maximizes the machine's travel range. Next, it is crucial to adjust the tool's position relative to the substrate, ensuring it is centered as previously described. Before securing it properly, the tool is centrally aligned with the rectangular slot in the fixture system to ensure that the additive material, when deposited, is centered with the tool's contact width. Figure 3.6 a) shows the tool mounted and aligned with the fixture system.

The tool maintains its position relative to the spindle, rotating about its own axis and moving vertically to adjust its depth during the test. Figure 3.6 b) illustrates the tool mounted on the milling machine.

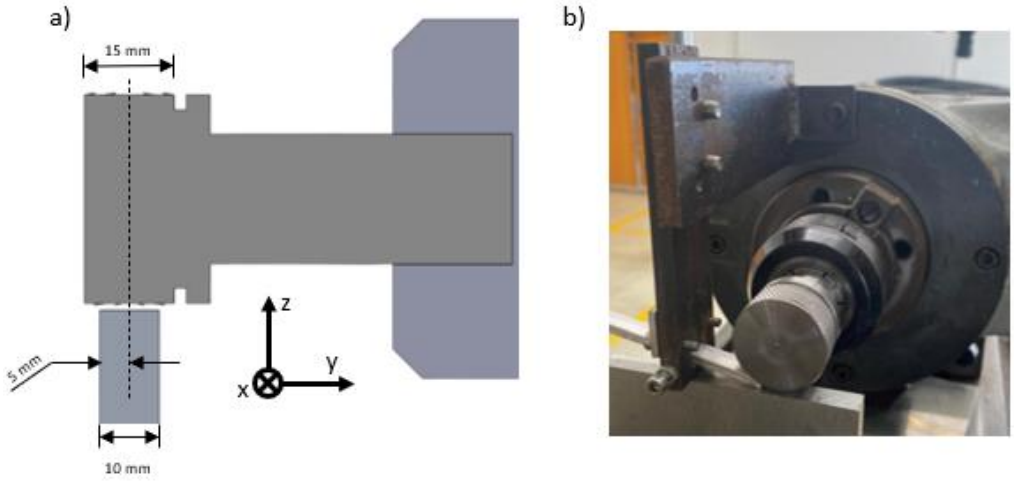

Figure 3.6 - Tool for FRAM tests: a) 3D modeling of the tool position; b) Tool setup on the milling machine.

One of the issues encountered during the initial tests was that, during deposition, the feeding material tended to deviate from the intended path, spilling over the substrate, as shown in Figure 3.7.

To address this problem, a plan was developed to secure the feeding material, which involved creating a guiding system to accommodate it. Additionally, the positioning and clamping of the substrate were improved using a bench vise fixed to the milling machine's work table. The assembly procedure was adjusted to include the positioning and adjustment of the guiding system based on the geometry of the feeding material.

Figure 3.7 - FRAM test with additive material deviation
viewed form orthogonal and top view.

To carry out the FRAM tests, an initial analysis was performed to determine the parameters that best suited the process. According to [10], the parameters that resulted in the most efficient deposition and bonding between layers were as follows: $\omega = 1000$ rev/min, $h = 0.7$ mm, and $\upsilon = 100$ mm/min.

For the tests conducted, parameters that closely resembled those previously mentioned were used. This adaptation was necessary due to the limitations of the machine, which only allowed selection of rotational and feed speeds according to the machine's range of options. The parameters used in the FRAM tests are summarized in Table 3.4.

Table 3.4 - Operational parameters of the FRAM tests conducted.

Rotational speed	Transverse speed	Tool penetration
900 rev/min	90 mm/min	0,7 mm

3.4.2 FRAM Tests with ceramic particles incoporation

When conducting the FRAM trials with the insertion of particles, additional preparations were required for the proper functioning of the process. In the tests carried out, four Particle Insertion Method (PIM) were used, varying the particle placement zone as well as the geometry adopted for the feeding material. In PIM1, a quantity of particles was placed on top of the already deposited layer, followed by the deposition of a new layer over them. In PIM2, it was necessary to fill the tube with particles before conducting the tests. In PIM3, the process was identical to PIM1, with the difference that the particles were placed on top of the feed material. In PIM4, a V-shaped profile was used for the feeding material, where the quantity of particles placed along its entire length was approximately 0.4433 g, with the possibility of variation. To obtain this profile, after cutting the plates to size, they were bent at a 45º angle. Figure 3.8 outlines the four strategies used in the various tests carried out.

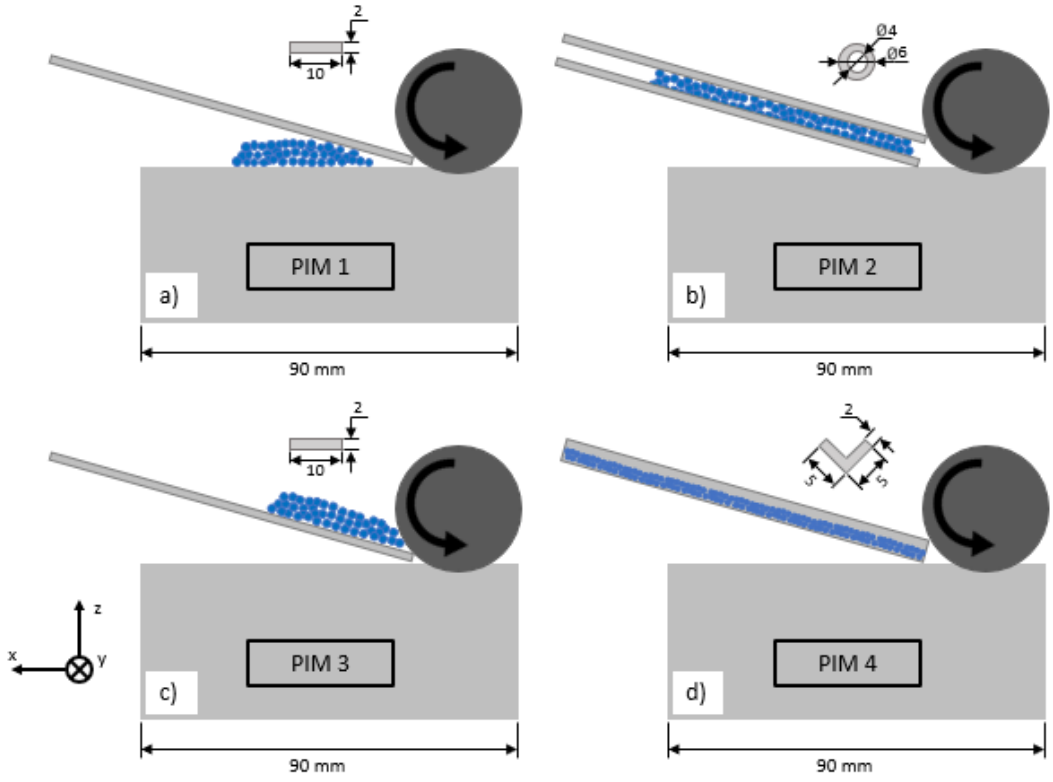

Figure 3.8 – Diagram of the particle insertion methods used during the FRAM tests: a) particles underneath a 10 × 2 bar; b) particles inside a tube; c) particles on top of a 10 × 2 bar; d) V-shaped bar with particles.

After conducting the trials with the insertion of ceramic particles, a problem was identified: during the deposition of particles along with the feeding material, excess particles that did not penetrate into the material fell by gravity around the deposition area. To address this issue and reduce particle waste, as well as to provide a safer and cleaner working area, an aluminum box was designed and implemented to enclose the substrate. This component is represented in Figure 3.9, mounted on the substrate after it was secured in the lathe.

Using a 10 mm thick and 155 × 103 mm aluminum AA5083 plate, this component was produced through machining and milling. It was manufactured with two roughing operations: a 30 mm diameter endmill was used to create the larger recess, and the external finishing with a 45º bevel and the slot where the substrate would enter was made with a 6 mm diameter endmill. For each trial involving the insertion of particles, it was necessary to mount this box on the substrate.

Figure 3.9 - Aluminum box for particles fitted into the substrate on the milling machine.

In these trials, two additional parameters were introduced that also influenced the deposition and dispersion of the particles during the experiment: the number of passes per layer, n, and the depth of each repeated pass per layer, d_{pass}. The operational parameters of the FRAM process for particle insertion are described in Table 3.5.

Table 3.5 - Operational parameters of the FRAM tests with particles insertion conducted.

Rotational speed	**Transverse speed**	**Tool penetration**	**Number of passes per layer (n)**	**Depth of the repeated pass (d_{pass})**
900 rev/min	90 mm/min	0,7 mm	1 / 2	1,4 / 2,1 mm

3.4.3 Schematics and process parameters

For the successful execution of all tests conducted with different parameters and objectives, a representative diagram of the various stages during the production of a wall by FRAM was outlined. Initially, as represented in Figure 3.10, the first two stages are necessary and sufficient for producing a wall by FRAM. In the first stage, the tool is set to rotate at the speed and depth defined in Chapter 3.4.1. Next, in the second stage, the process remains identical for the remaining layers, adjusting the tool height for each layer if needed. Table 3.6 lists all the tests performed under these conditions, referenced by codes and defined with a primary objective for each.

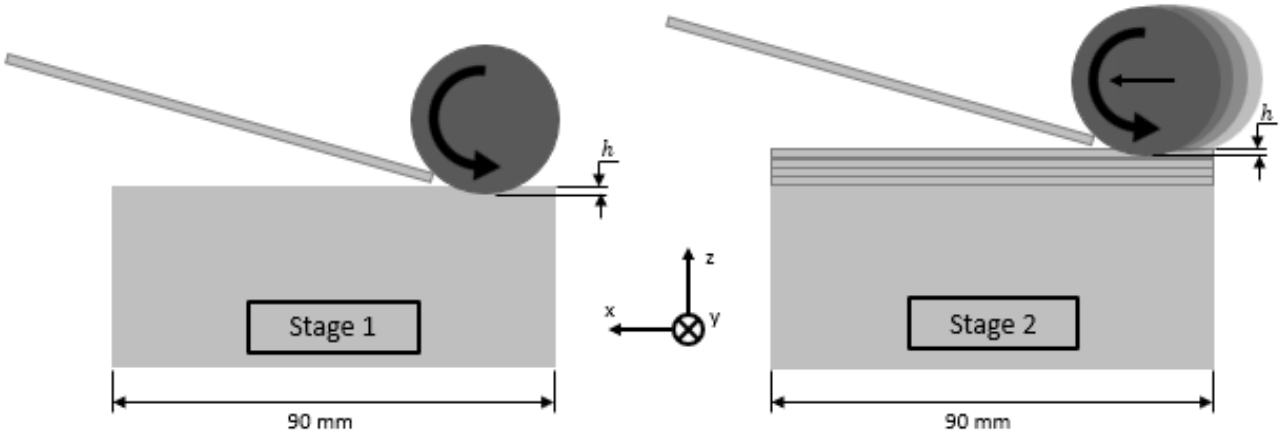

Figure 3.10 - Different stages for the production of walls by FRAM.

Table 3.6 – FRAM tests conducted.

Test name	Code	Total Layers	Objective
Test with thin Bar 8	TBAR8	8	Test the parameters of the process and the geometry of the feeding material
Test with thin Bar 65	TBAR65	65	Wall with dimensions to withdraw specimens
Test with Tubular Section inner diam. 4mm and exterior diam. 6mm	TTUBE	5	Test the behavior of the tubular section
Test with Squared Section 6 × 6 mm	TSQUARE	9	Test the behavior of the squared section

Entering the FRAM tests with particle insertion, the production process involved some additional stages. For each such test, it was necessary to perform the first two stages, if the purpose is to produce layers without particles, previously mentioned for the production of layers without particles. Then, when the goal is to produce walls with particle zones, two more stages were required, represented in Figure 3.11. The first additional stage (Stage 3) involved the deposition of the feed material with particles, as explained in Chapter 3.4.2, with the tool positioned at the defined deposition depth. Next, in Stage 4, the tool was adjusted to the repeated pass depth (d_{pass}), meaning an additional pass over the deposited layer was necessary to improve the consistency and uniformity of the particles within the feed material. In this same step is represented the possibility of performing multiple passes per layer, represent with n, depending on the operator's objective, with multiple passes being a significant factor in the mixing and dispersion of particles.

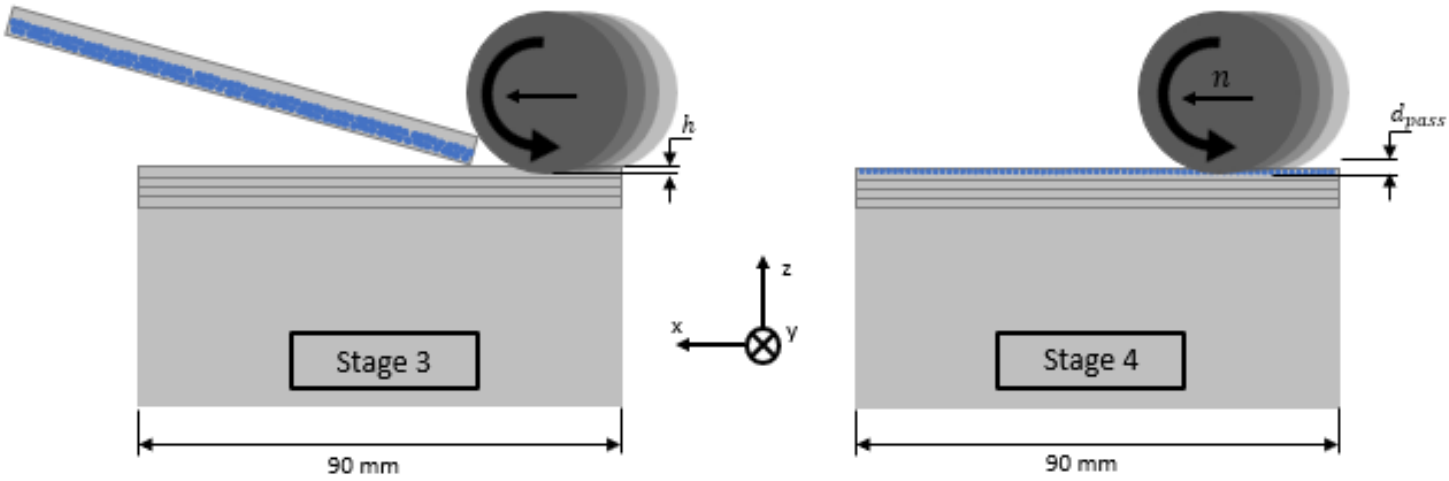

Figure 3.11 - Different stages for the production of layers by FRAM with insertion of particles.

In Table 3.7, all the FRAM tests with particle insertion are represented, showing the two main parameters operated during the layers with particle deposition.

Table 3.7 - FRAM tests with particles insertion conducted.

Code	Strategy	Layers with particles	Number of passes per layer with particles (n)	Depth of the repeated pass (d_{pass})	Total Layers	Objective
TP7	Figure 3.8 a) and b) (test being conducted here)	6	-	-	22	Test different geometries and insertion types
TP8	Figure 3.8 b) and d)	6	0 1 2	1,4 mm 2,1 mm	33	Test the parameters n and d_{pass}
TP9	Figure 3.8 d)	3	2	1,4 mm	58	Wall with particles with dimensions to withdraw specimens
TP10	Figure 3.8 d)	1	-	-	6	Test wall flattening
TP11	Figure 3.8 d)	1	1	1,4 mm	6	Test wall flattening
TP12	Figure 3.8 d)	1	2	1,4 mm	6	Test wall flattening
TP13	Figure 3.8 d) (test being conducted here)	6	2	1,4 mm	28	Obtain wall zone with particles

3.5 Characterization of walls produced by FRAM

This subsection outlines the various characterization techniques employed to evaluate the physical properties of samples produced by FRAM. Figure 3.12 illustrates the areas from which each sample for the different types of characterization was extracted, ensuring accurate interpretation of the analyzed regions and subsequent discussion of results. The samples for tensile testing were also taken from walls with inserted particles for future comparison of results.

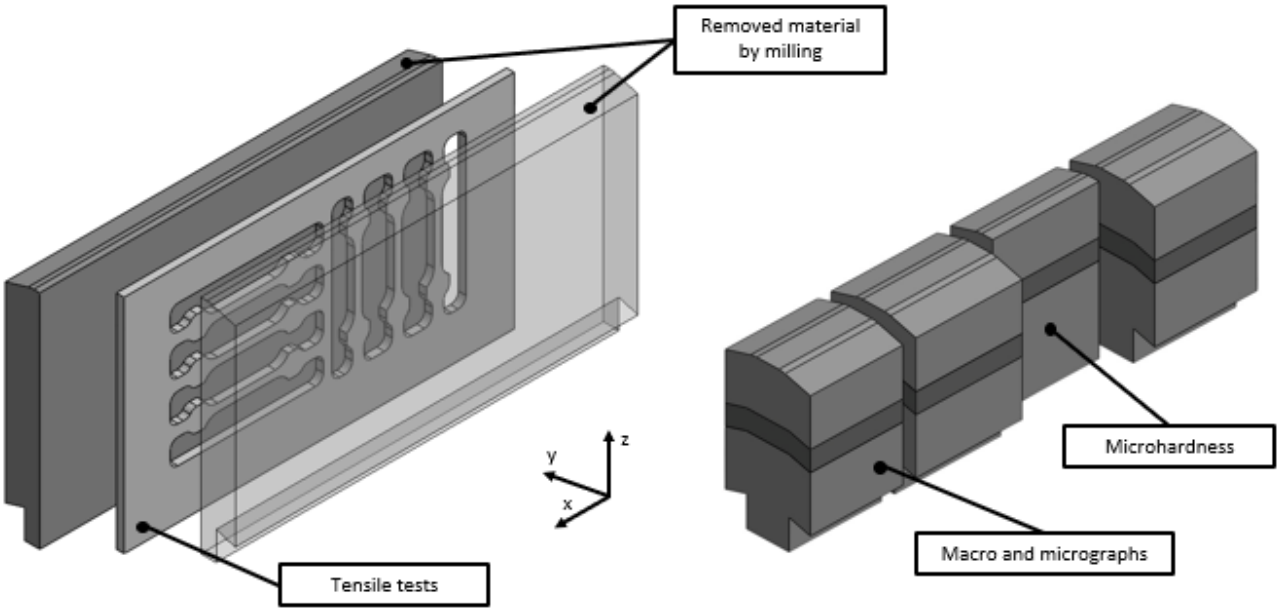

Figure 3.12 - Schematic illustration of the samples and their placement within the tests conducted for different characterizations

3.5.1 Metallographic characterization

To analyze the macrostructure and particle distribution, a macrostructural analysis was conducted on various samples produced with particles using the FRAM process, using an Olympus CX40 optical microscope. Macrographic images were compiled using the AutoStitch tool, which stitches overlapping photos together, combining multiple images taken with a x5 magnification lens.

For a better macrographic analysis of the particle location and dispersion, as well as the interface between layers, all particle samples were embedded in a Keller's reagent solution, whose chemical composition is described below, according to the literature [26]:

- Distilled Water - 175 ml
- Hydrochloric Acid (HCl) - 3 ml (37%)
- Nitric Acid (HNO_3) - 20 ml (65%)
- Hydrofluoric Acid (HF) - 2 ml (48%)

Following this, the microstructure and particle distribution in specific areas of each sample were analyzed and characterized, such as the particle deposition zone in the center of the samples and the boundary region between the substrate and the first layer, using the previously mentioned optical microscope. All samples were prepared by sequentially using sandpapers of different grits (P80, P240, P320, P400, P600, P1200, P2500, and P4000), followed by polishing with 0.3 µm alumina.
Subsequently, the fracture surface of the tensile-tested specimens was analyzed using SEM to interpret the type of fracture and the behavior of layer interconnections in the different tests.

3.5.2 Uniaxial Tensile Tests

Uniaxial tensile tests were conducted at room temperature using an StepLab EA05 (Figure 3.13 a)), with a capacity of 20 kN, according to the ASTM E8/E8M-13a standard. To machine the test specimens, the results of the tests were faced on both sides to ensure a uniform thickness, t, of 2.5 mm. The specimens were then machined from the samples using the HAAS Super Mini Mill 2 CNC machining center. Figure 3.13 b) shows the technical drawing of a test specimen for tensile testing.

a)

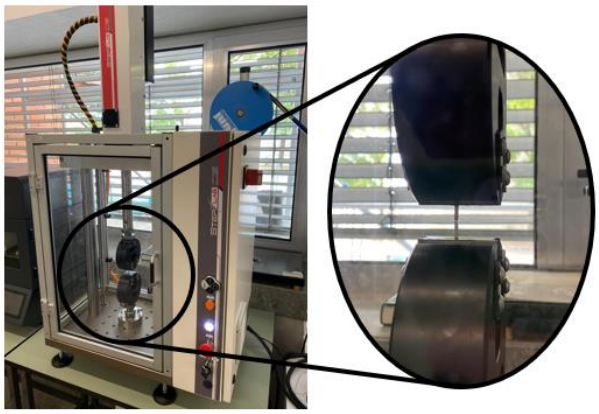

b)

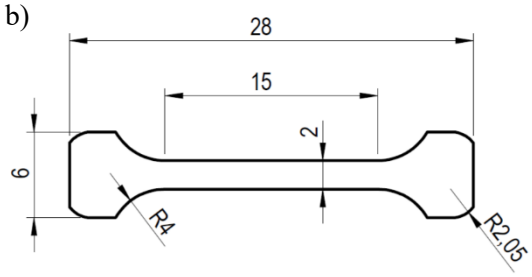

Figure 3.13 – Uniaxial Tensile Tests: a) Equipment used; b) Technical drawing of the tested specimens.

From these tensile tests, columns of values for force (N) and elongation (mm) were recorded for each test. The value l_0, which is the initial length, is the distance between the clamps of the machine. To create a comparative method within the International System (IS), the values were converted to Engineering Stress (σ) and Engineering Strain (ε), respectively. This required processing the data using the following equations:

$$\varepsilon = \frac{l - l_0}{l_0} \qquad (1)$$

$$\sigma = \frac{F}{A_0} \qquad (2)$$

3.5.3 Hardness mapping

After the preparation indicated for this type of analysis, the Vickers hardness map was obtained along the longitudinal width of the samples (x-axis) using a Mitutoyo HM-112 hardness machine. The samples used are shown in Figure 3.12, where the cross-sectional surface was analyzed.
Three lines of indentations were made in each test, with a load of HV0.3, spaced 2.5 mm apart in the x-direction. Throughout the processed area, the indentations were made with a distance of 2.5 mm in the y-direction.
This hardness analysis was conducted to compare the processed area with the non-processed area, as well as to evaluate the influence of the particles on the walls manufactured by FRAM.

3.5.4 Thermographic analysis

For all FRAM experiments conducted, the temperature of the substrate and the tool was measured during the process. An infrared thermographic camera, Fluke Ti400, was used, fixed at the end of the milling machine table, pointed and properly calibrated at a distance of approximately 54 cm from the process. To obtain the thermographic results, the Fluke Connect software was used to capture the temperature scales and variations during the tests. To analyze the test during its execution, an emissivity of 0.99 was set, and the substrate was pre-coated with matte black paint to prevent reflections from the aluminum.

The purpose of using the camera for temperature measurement was to determine the temperature reached at the interface between the tool and the substrate, to understand the temperatures to which both are subjected and the possible consequences on material deformation during the process. It was also used to monitor the temperature of the substrate to ensure it did not exceed the melting temperature of Aluminum. Throughout this dissertation, the different tests conducted will include an attachment with a hyperlink to the video recorded by the thermographic camera during the test.

4

EXPERIMENTAL RESULTS

This chapter provides a description of all the experimental tests conducted, as well as the characterization performed according to the type of test conducted.

The initial tests were considered preliminary as they aimed to test the parameters optimized by the literature for the process and to adjust the profile of the feed material to observe how different profiles behaved during the process. After these tests, some adjustments were made to the tool position and the feed material holder.

Subsequently, larger walls were fabricated to extract samples for tensile tests. Additionally, FRAM tests with ceramic particles were conducted. These particles were inserted using different methods in various tests, and through matrix organization, the number of passes per layer with particles and the depth of each tool pass relative to the last deposited layer were tested.

All these tests underwent a more detailed analysis, which included the following characterization techniques: macro and microscopic analysis of the cross-sectional and longitudinal views with and without contrast, hardness tests, and SEM analysis. Throughout all the tests, the temperature variation during the process was monitored using an infrared thermographic camera.

4.1 Production of walls by FRAM

Initially, experimental tests were conducted without ceramic particles. The main objective was to adjust the most suitable feed material profile for deposition in the FRAM process. As the first preliminary test (Figure 4.1), a wall was produced by FRAM using the parameters defined in Chapter 3.4.1 and rectangular aluminum strips measuring 10 × 2 × 100 mm. The produced wall was then cut into three different zones, transversely, for comparison of the beginning, middle, and end of the deposition during the process, as shown in Figure 4.3.

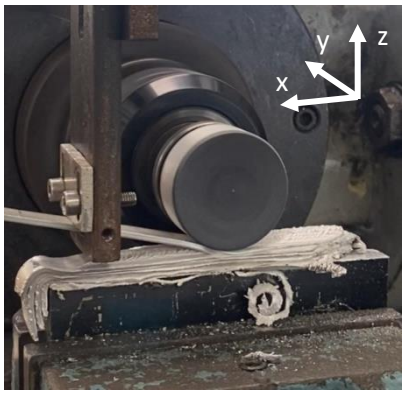

Figure 4.1 – TBAR8 test being conducted. The test being conducted can be found here

During this test, a thermographic analysis was performed using the equipment mentioned in sub-chapter 3.5.4, with the corresponding link in Figure 4.2, representing the three different phases of the process: the beginning of deposition (Figure 4.2 a), the middle (Figure 4.2 b), and the end (Figure 4.2 c).

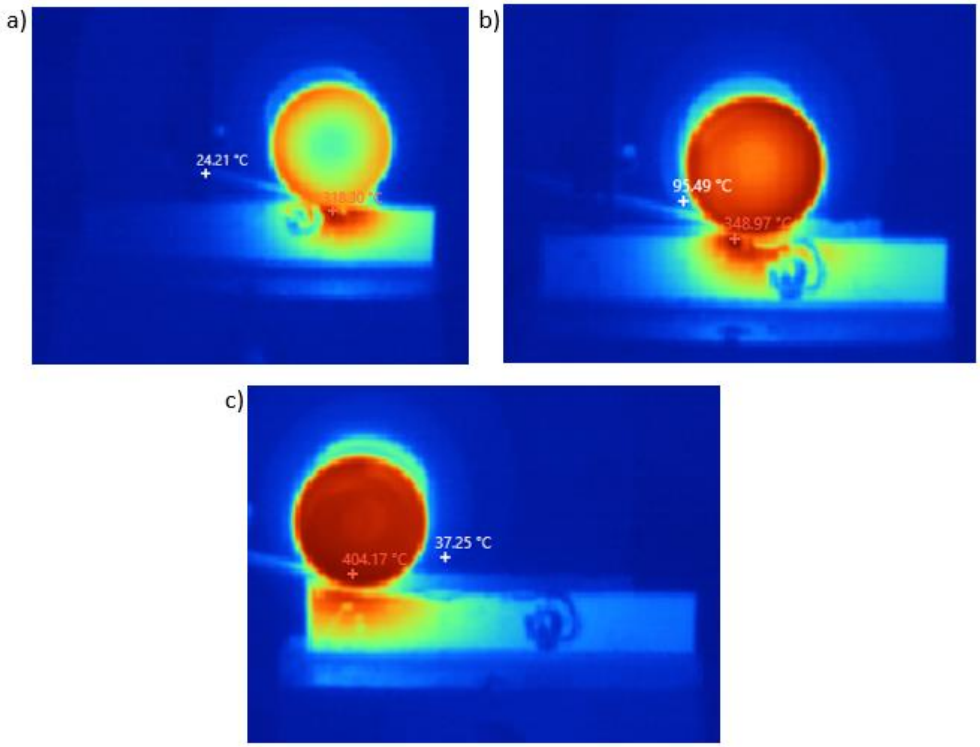

Figure 4.2 - Thermographic analysis results of the TBAR8 test in the different deposition zones: a) beginning; b) middle; c) end. The full thermographic analysis can be found here

It can be observed that the contact zone between the tool and the base material is the area with the highest temperature, due to the frictional movement. Throughout the deposition process, a considerable increase in the tool's temperature can be observed, resulting from the mechanical stresses it undergoes.

During the process, the deposition zone of the added material reaches temperatures between 318-350ºC, the value varies between these two limits, increasing as the tool progresses during deposition. These temperatures which may rise due to the tool heating up over time. These temperatures are ideal for the deformation and bonding of the aluminum layers. It is also noteworthy that there is no excessive heat accumulation in the substrate, preventing any damage to it.

Figure 4.3 represents the result of the TBAR8 test. For a visual comparative analysis at different stages of the test, the results of the TBAR8 test obtained from the transverse cut of the different parts of the test are presented in Figure 4.3 a), b) and c).

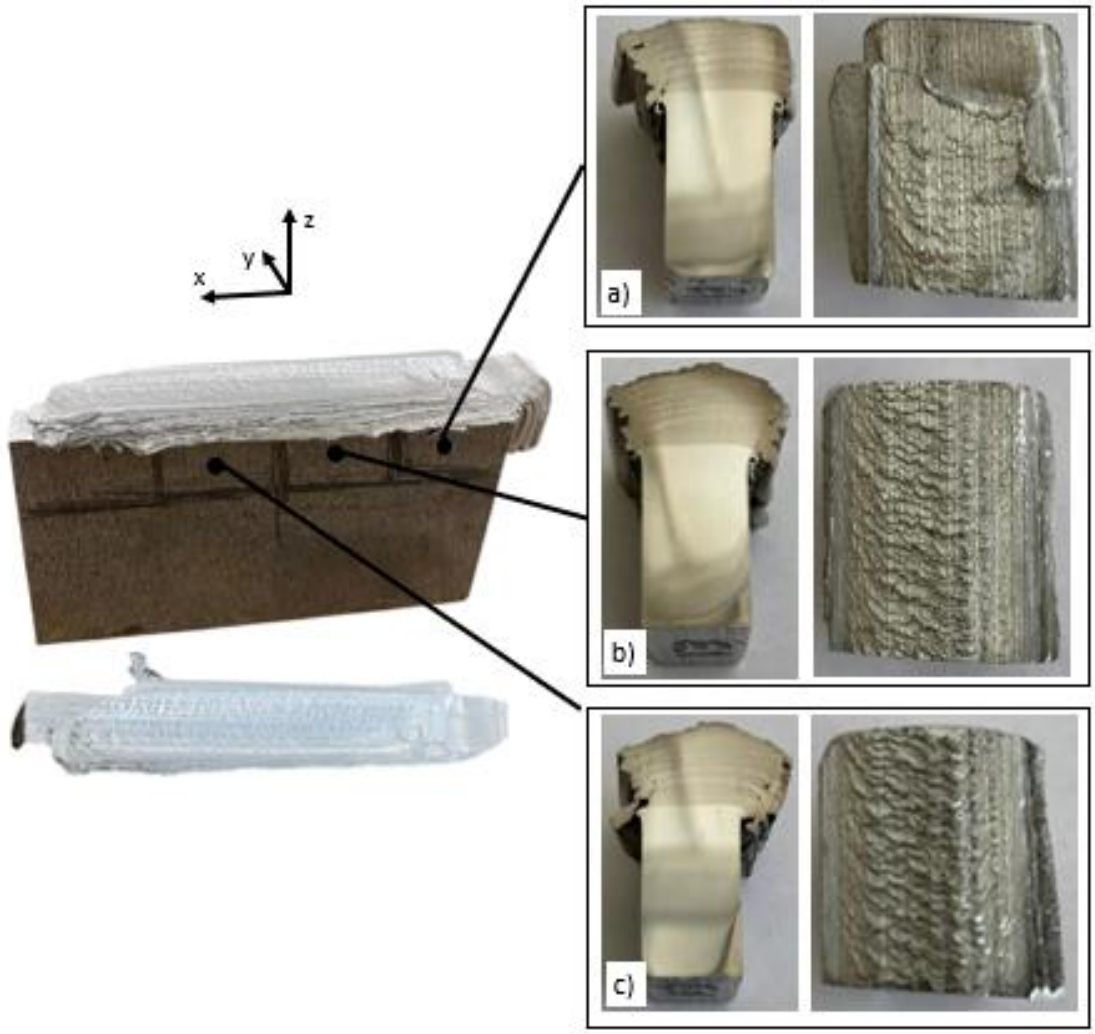

Figure 4.3 – Final result of the TBAR8 test with the different cut zones marked: a) beginning of the wall; b) middle of the wall; c) ending of the wall.

As observed, during both phases of the wall, there was a complete deposition of the feeding material, with complete interlayer bonding, resulting in a relatively smooth and uniform surface. It can be seen that the final part of the wall exhibits some surface irregularities. This is due to the tool's movement over the substrate; as less material remains to be deposited, the tool becomes more unstable, leading to a poorer deposition quality. For a more detailed analysis of the material distribution along the length, a longitudinal cut was performed, in the beginning of the test result, as shown in Figure 4.4.

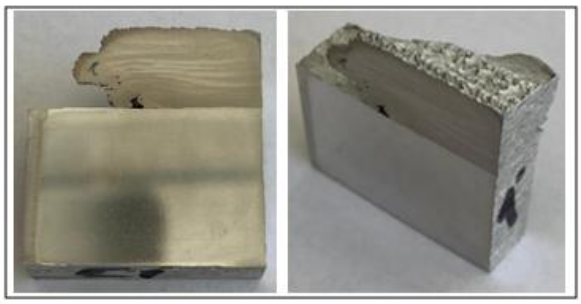

Figure 4.4 - Visual analysis of the longitudinal section at the beginning of TBAR8.

It can be confirmed that the layer deposition occurred, but with the particularity that along the length, the interlayer bonding was not uniform, with a noticeable wave-like pattern in the layer deposition.
Following this, two additional preliminary tests were conducted, where two types of profiles for the feeding material were tested. The goal was to observe their behavior under the parameters initially used in TBAR8. Figure 4.5 represents the results for these two tests

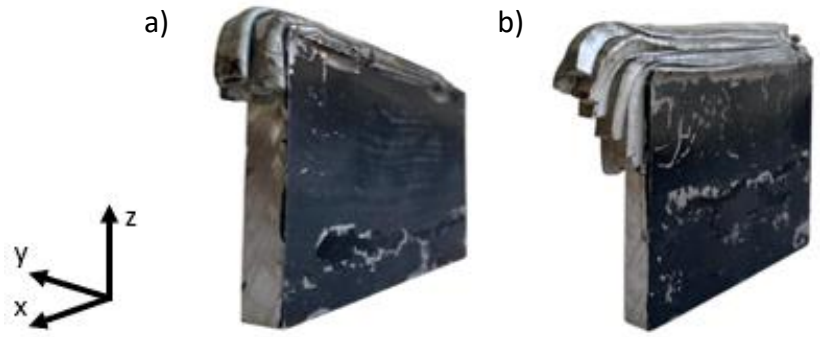

Figure 4.5 – Test results of: a) TTUBE (video of the test here); b) TSQUARE (video of the test here).

The results obtained from these two tests are presented in Figure 4.6, where a qualitative analysis of the surface finish was performed, compared to the results of TBAR8 test.

Figure 4.6– Final results of the profile variation test with: a) square section (TSQUARE); b) tubular section (TTUBE).

We concluded that, with these two profiles, the visual results are identical to those of TBAR8 test. However, both tests revealed some disadvantages concerning surface finish, burr, and experimental procedures. It was concluded that these profiles have a defect on the production of walls using FRAM, which is the accumulation of material at the center of the deposition, resulting in a non-uniform distribution across the width. In the test with the tubular section, a poor interlayer bonding at the end of the wall was also observed due to the hollow profile.

Following these previous tests, we proceeded to the main tests, opting to use thin metallic strips of 10 × 2 × 100 mm for a new experiment. The primary objective of this test was to achieve the maximum high of the wall produced, which was 65 layers, to extract specimens for tensile testing. The setup and experimental apparatus for the TBAR65 test are shown in Figure 4.7. This test aimed to analyze the behavior of the overlapped layers after a period of time, subjected to the accumulated heat during the process.

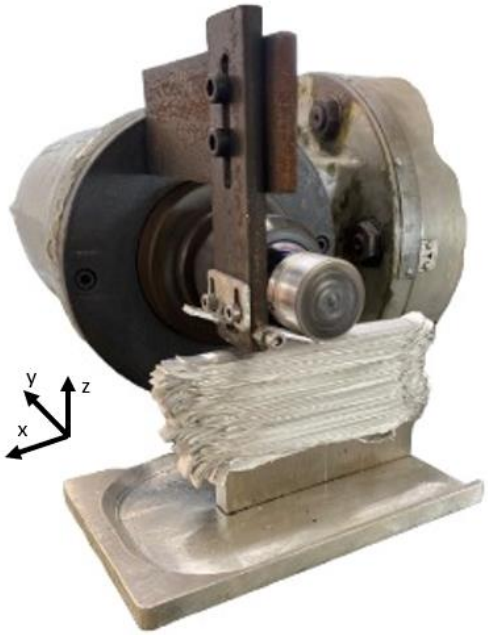

Figure 4.7 - Experimental setup during the TBAR65 test. Teste being conducted here.

This test was conducted using the same parameters previously defined, with the specific exception that every 10 layers, a pause of approximately 30 minutes was implemented to prevent the machine from overheating. A total of 65 layers were deposited in this test, resulting in a wall with dimensions of 60 × 90 mm, as shown in Figure 4.8. To prepare the wall for the extraction of specimens for tensile testing, the faces of the wall were machined down to a thickness of 5 mm in the center, as this was the area of interest where greater uniformity in layer bonding was observed.

Figure 4.8 – Front and top view of the final result of the TBAR65 test.

Through the analysis of the final produced wall, it is possible to observe a surface that is smoother compared to TBAR8 (Figure 4.3). This improvement is likely attributed to the wall being subjected to more temperature cycles and a greater overlap of layers, which made the deposition more uniform and the surface quality more desirable.

4.2 Production of walls by FRAM incorporating ceramic particles

After optimizing and standardizing the FRAM process through various tests, experiments were conducted incorporating ceramic particles, and the parameters influencing their deposition and dispersion were optimized.

In order to test the influence of repeated passes per layer, three tests were conducted with three different sets of parameters, named TP10, TP11, and TP12. The parameters used as well as the objectives are outlined in Table 3.7. The experimental setup used during this process is represented in Figure 4.9 a). In each test, a total of 6 layers were deposited, with the last layer including particle insertion. This layer is shown being deposited. The side and top views of the three produced walls are represented in Figure 4.9 b) to d).

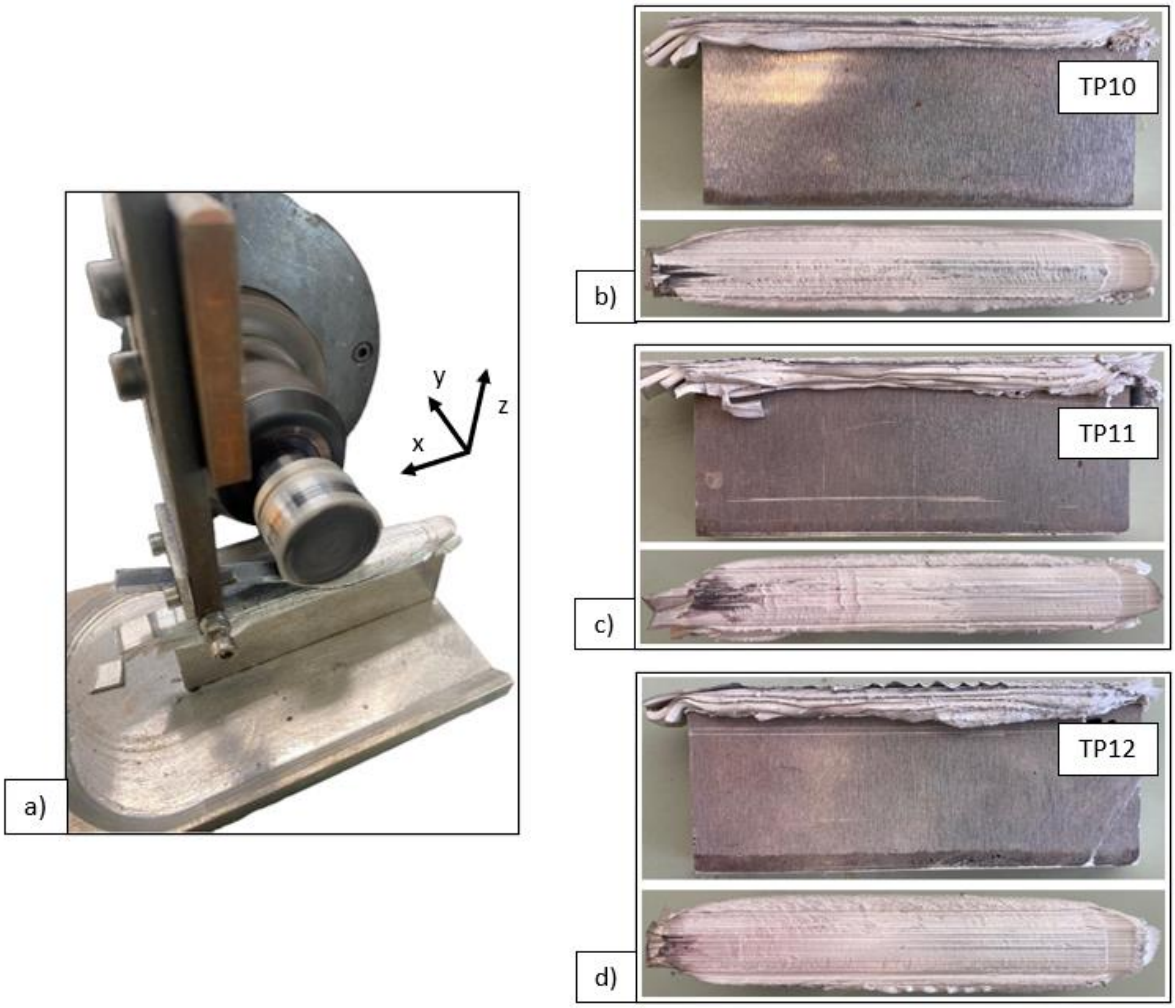

Figure 4.9 - a) Experimental setup and results of the tests: b) TP10; c) TP11; d) TP12.

It was concluded that as the number of passes over the deposited layer with particles increased, the wall tended to become flatter. There is a noticeable difference between TP10 and the other two tests, with a less abrupt difference between TP11 and TP12. This indicates that from one to two passes, there is not a significant flattening of the wall. In the thermographic analysis, an increase in the temperatures of the processed area was observed during repeated passes, which was expected due to the preheating from previous passes. This flattening caused by the repeated passes is directly related to this temperature increase, leading to more pronounced deformation of the already deposited layers. In other words, as the number of passes increases, more temperature cycles are accumulated in the material, leading to greater deformation.

From the top views, it was concluded that the more passes made, the more uniform and less rough the surface becomes. Additionally, particle dispersion and accumulation on the surface were noted. In TP10, without any repeated passes, particles in large quantities can still be observed on the wall's surface, whereas in TP12, the surface is almost completely free of particles. This fact was better illustrated through optical microscopy imaging later in this dissertation.

In conclusion, multiple passes on a single layer influence the height of the produced wall, and this fact should be considered when producing walls with specific dimensions.
In order to test different geometries and particle insertion methods to find which one is the most efficient, the TP7 test was conducted. The main objective was to make a comparative analysis between two particle deposition techniques with different geometries.
In the three upper layers, shown in Figure 4.10 a), a tubular section feeding material was used, filled with particles occupying about 75% of its total volume. In the three lower layers, shown in Figure 4.10 b), particles were deposited by placing a specific amount at a localized spot in the tool path, underneath the feeding material (thin plate).

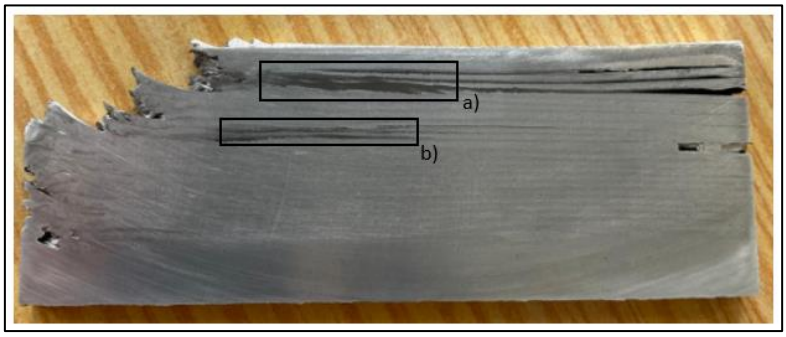

Figure 4.10 – Final result of the TP7 test: a) tubular section used; b) thin plate used.

We concluded that in the layers where thin sheets with particles inserted underneath were used, there was an accumulation of particles in the zone where they were deposited, with no longitudinal dispersion, as well as an increase in temperature in the mixing zone of the particles with the base material. In contrast, using the tube resulted in a greater longitudinal dispersion of the particles. In both cases, the number of inserted particles was excessive, which is a factor to be controlled and reduced in future tests. It was also noted that in the layers made with the tube, towards the end of the deposition, there was no complete interlayer bonding, as seen in Figure 4.10.
In conclusion, a strategy to disperse the particles must be adopted. This could involve modifying the geometry of the thin sheet by bending it and inserting particles along its entire length, as was done in tests TP10, TP11, and TP12.

In order to determine the optimal parameters for particle deposition, an experiment (TP8) was conducted to test various combinations of parameters that directly influence particle deposition. Several combinations were made, with the two parameters tested being the depth of the repeated pass and the number of passes per layer with particles. For the first parameter, depths of 1.4 mm and 2.1 mm were tested, and each of these was then combined with different numbers of passes per layer (n=1, 2, or 3).

By visual analysis, it was not possible to conclude which parameters would be the most suitable for the deposition of layers with particles.

After conducting these tests, a new experiment was carried out with the objective of producing a wall featuring a central zone of particles. In this case (TP13 test), this was achieved with 6 central layers using the parameters described in Table 3.7. The experimental setup was identical to the previous tests. The final result of the test is shown in Figure 4.11.

Figure 4.11 - Final result of TP13 test.

To study the different zones of interest, transverse cuts were made to extract two sections of the TP13 test for analysis of the transverse and longitudinal surfaces. Figure 4.12 a) shows the cuts made in the TP13 test. After machining the two extracted samples, they were properly faced and polished for various analyses and characterizations throughout this dissertation. These samples are shown in Figure 4.12 b). Some visual conclusions that can be drawn are that, in both the transverse and longitudinal views, there appears to be complete interlayer bonding, even with the presence of particles. One noteworthy observation is that in the particle zone, the particles did not disperse between layers, remaining in a line, and it was not possible to achieve a fully dispersed particle zone as expected.

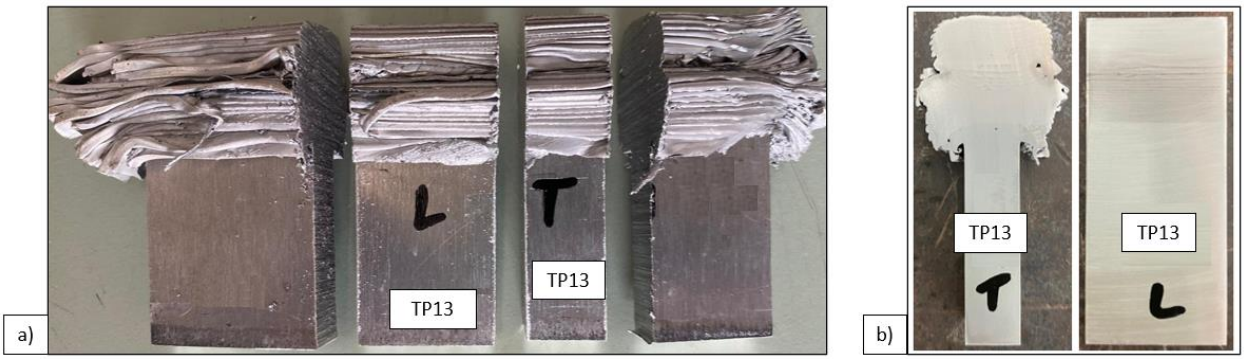

Figure 4.12- Representation of the cuts made in the test: a) before machining; b) after machining and polishing.

Finally, a last test (TP9) was conducted with the aim of producing a wall significantly larger than the previous ones, in order to accommodate samples. Three layers of particles were deposited in the center to ensure their presence in the samples for subsequent tensile testing. The experimental setup was identical to that of the previous tests, with each particle layer having the following parameters: d_{pass} = 1.4 mm and n = 2. In Figure 4.13 a), the final result of the test was shown. Figure 4.13 b) shows the wall after the machining, to take the samples for tensile tests.

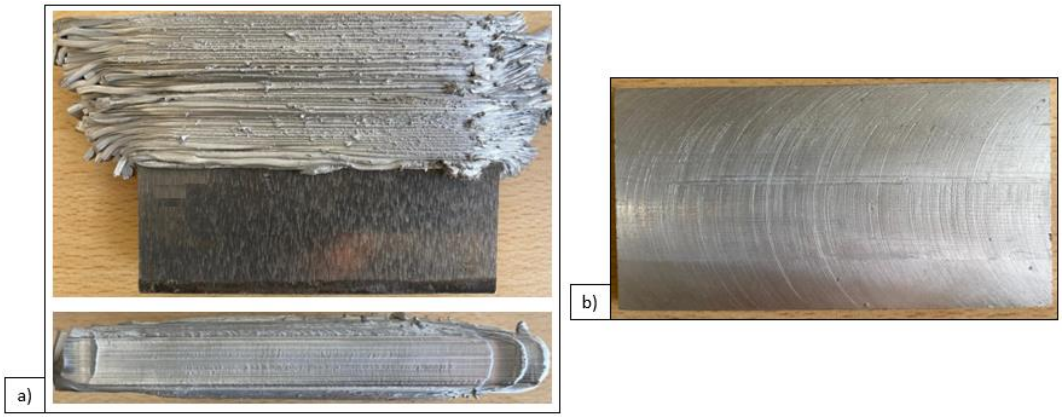

Figure 4.13 - TP9 test conducted a) before machining; b) after machining.

4.3 Characterization of the samples

4.3.1 Metallographic characterization (Micro and Macrographic analysis)

The analysis of particle distribution in the surface zone of the three samples of the three tests (TP10, TP11, and TP12), as well as the height of each layer, was achieved using macrostructural and microstructural characterization techniques. For this analysis, a section was cut from each test to examine the cross-section. After all polishing steps, the face to be analyzed was treated with Keller's reagent, whose composition is described in chapter 3.5.1. Figure 4.14 shows the three samples taken from the three walls. Figure 4.15 represents the macro and micrographs of the TP10, TP11, and TP12 tests.

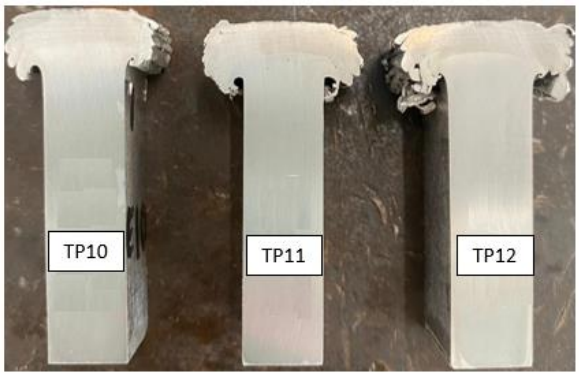

Figure 4.14– Cross-section samples taken from each test.

Through the analysis of Figure 4.15 a – c, it is possible to conclude that increasing the number of passes per layer indeed influences the flattening of the already deposited layers, which consequently affects the final height of the wall. We can observe that the last layer deposited in the TP10 test wall is approximately 1.17 mm, compared to the TP11 test, which is 0.98 mm, and the TP12 test, which is about 0.78 mm, resulting in a decrease of 16% and 35% in height. The same process is similar in the remaining layers below the particle layers.

In the layers without particles, it is possible to observe the transition zone mentioned earlier, identified as the darker area that separates the layers.

From Figure 4.15 a_2 - c_2, it is evident that without repeated passes in the particle layer (TP10 test), the particles tend to cluster in zones without deep dispersion, compared to the TP12 test. When comparing TP11 with TP12, it is noteworthy that to achieve a greater dispersion of the particles, at least two repeated passes per particle layer are necessary.

In the images with higher magnification, it is possible to observe the transition zones from the substrate to the first deposited layer. In Figure 4.15 b_4 the microstructure of the substrate is visible, but the microstructure of the added material is not. This is due to the fact that the Keller´s reagent is not suitable for the alloy series of the added material.

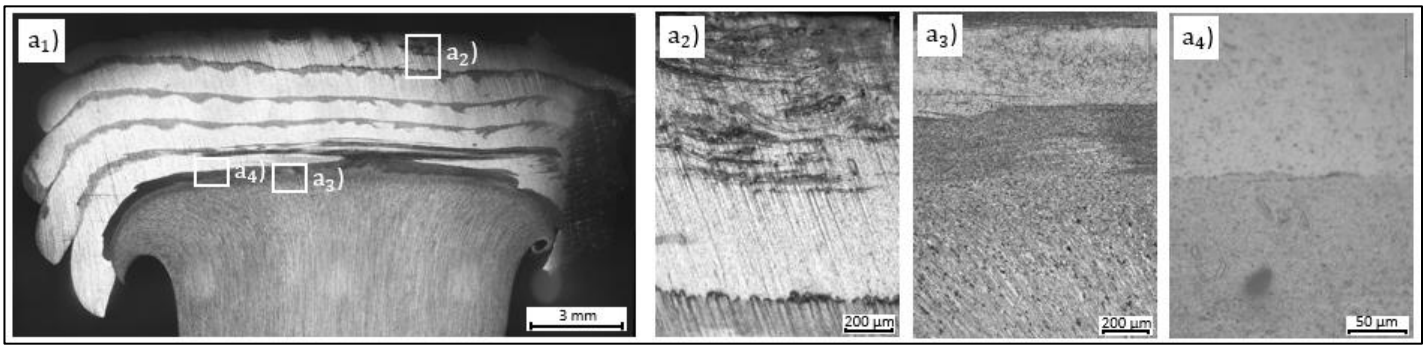

a) TP10

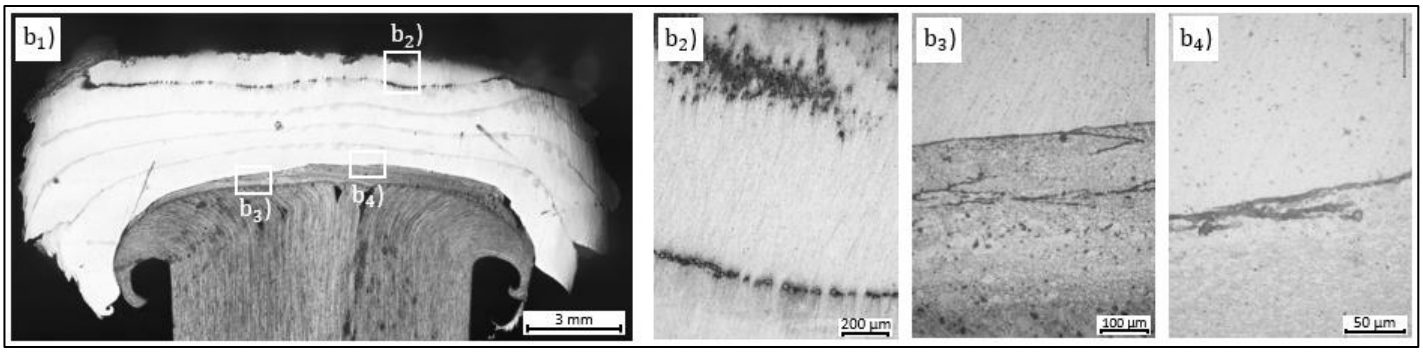

b) TP11

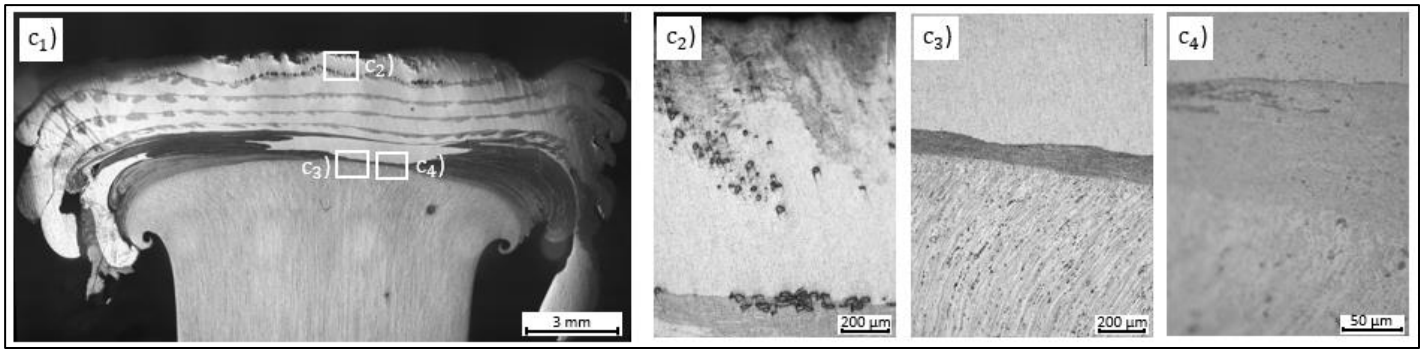

c) TP12

Figure 4.15 - Macro and microestrutural characterization of a) TP10, b) TP11 and c) TP12.

4.3.2 Uniaxial Tensile Tests

The mechanical behavior of the tests conducted by FRAM was evaluated using uniaxial tensile tests. From Figure 4.16 to Figure 4.18, the stress/strain curves of the conducted tests are represented.

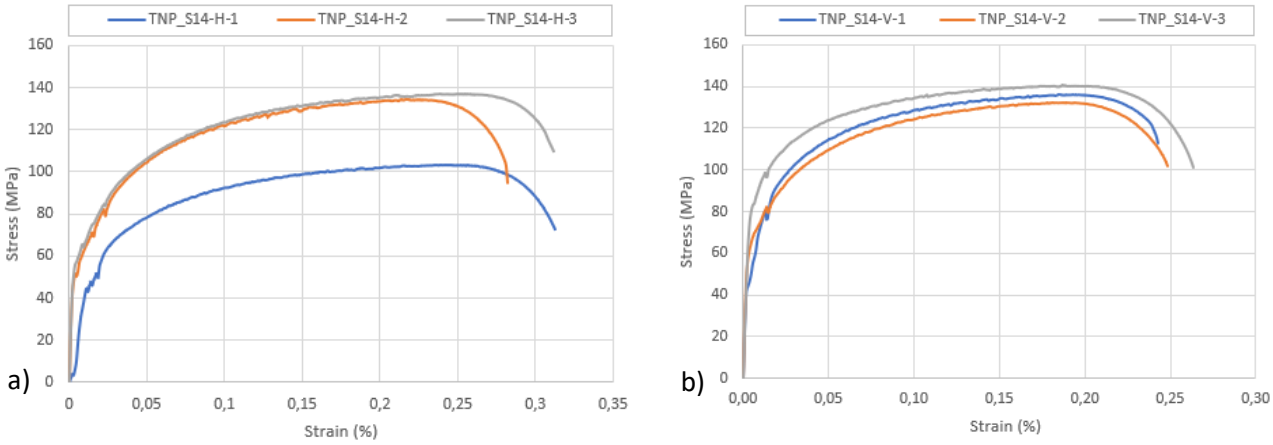

Figure 4.16 - Stress/strain curves of the uniaxial tensile tests of a) TBAR65-H and b) TBAR65-V.

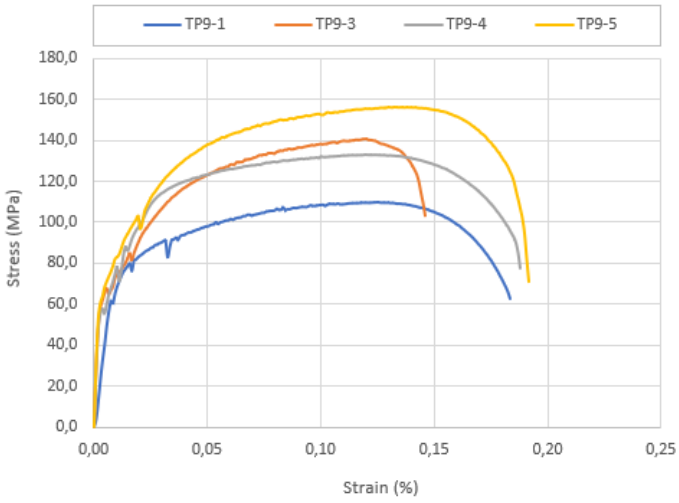

Figure 4.17 - Stress/strain curves of the uniaxial tensile tests of TP9.

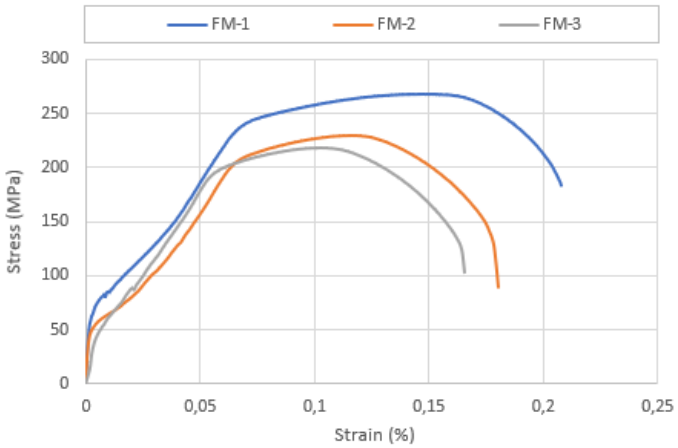

Figure 4.18 - Stress/strain curves of the uniaxial tensile tests of the Feeding Material (FM).

The most important mechanical properties for comparison between tests were organized in a bar chart shown in Figure 4.19.

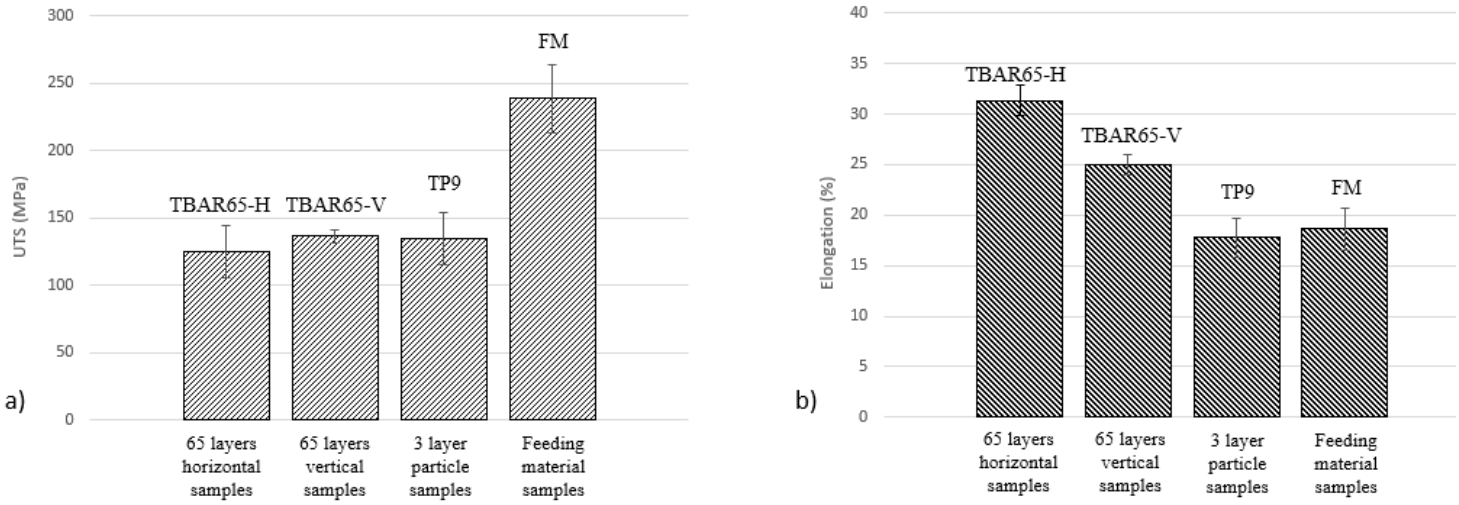

Figure 4.19- Comparison of a) UTS and b) Elongation of the samples taken from the different tests conducted.

By comparing the TBAR65-H and TBAR65-V tests, it was concluded that the UTS in the vertical direction was slightly higher than in the horizontal direction. However, the horizontal direction exhibited greater elongation, about 8.4 %, compared to the vertical direction (Figure 4.19), as expected according to the literature [2]. This phenomenon is attributed to the position of the specimens in the wall, where the vertical specimens experienced force perpendicular to the deposition of layers, leading to quicker rupture of these interlayer bonds than when the force was parallel to the layers, as in the horizontal direction. According to [2], this phenomenon might also be related to the finer grain size in the YZ plane compared to the XZ plane, as illustrated in Figure 2.12.

The UTS of the specimens from the FRAM process were higher than those from the processed material walls. This increase is attributed to the softening phenomenon caused by excessive grain growth and dissolution of strengthening phases at high temperatures [27]. This phenomenon often occurs in additive manufacturing processes for some aluminum alloys. However, considering the elongation of the addition material, it is noted that this value is lower compared to the processed material wall, concluding that the processed material wall achieved some degree of ductility and fracture resistance.

Comparing the TBAR65-V and TP9 tests, where the specimens were taken from the same position, it is possible to conclude that the UTS decrease 1.1%, that did not change significantly with the introduction of particles into the material. This suggests that particle addition did not compromise the strength of the produced wall. Nevertheless, the elongation recorded in the test with particles was lower than that in a wall without particles in the same vertical direction. This is due to the particles causing interruptions in the layer bonding at some points, which facilitated the rupture of these bonds.

4.3.3 Analysis of the Fractured Surface (SEM)

To analyze the fractographic behavior of the walls produced by FRAM, the fractured surface of one specimen from each tensile test was examined. From Figure 4.20 to Figure 4.23, the fractured surfaces of each specimen are shown, with great magnification on the right.

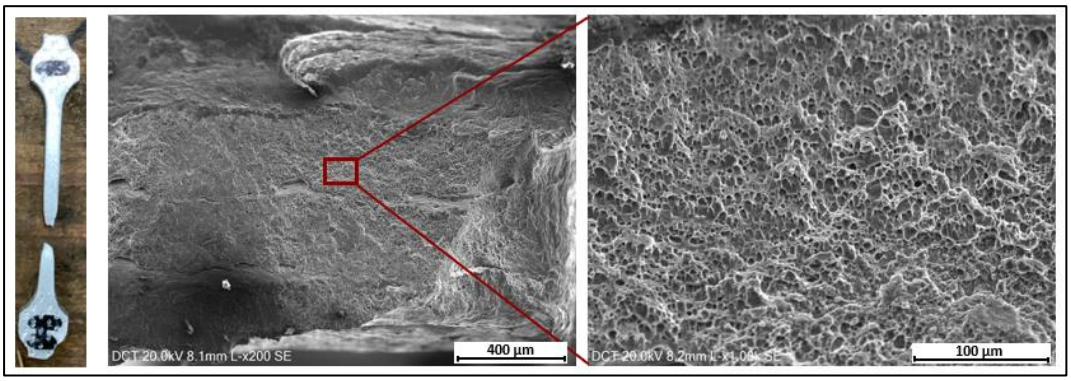

Figure 4.20 - Fracture sample and surface of the TBAR65-H test (sample Horizontal 1).

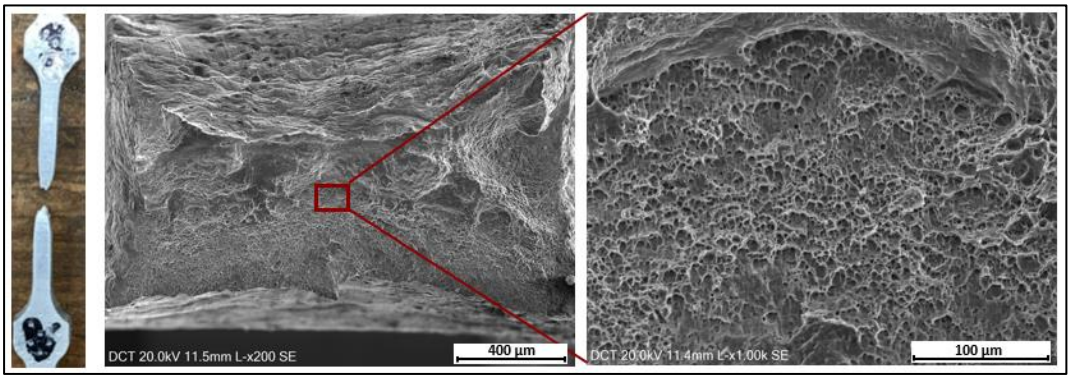

Figure 4.21 - Fracture surface of the TBAR65-V test (sample Vertical 1).

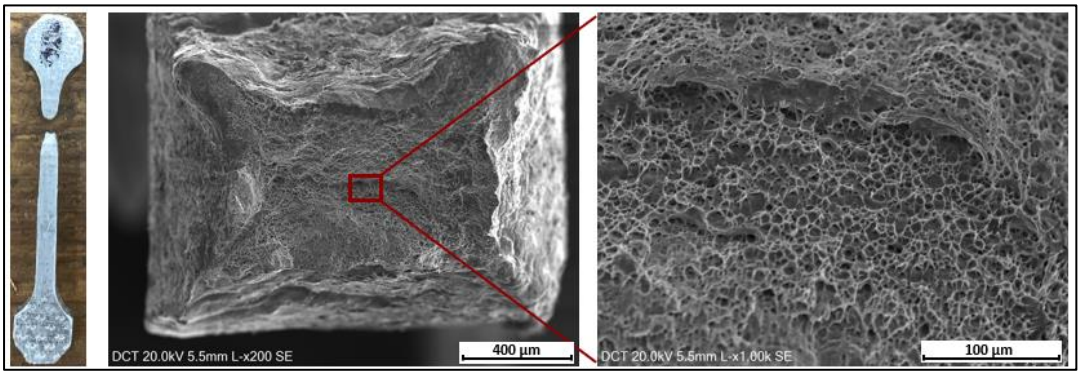

Figure 4.22 - Fracture surface of the sample TP9-1.

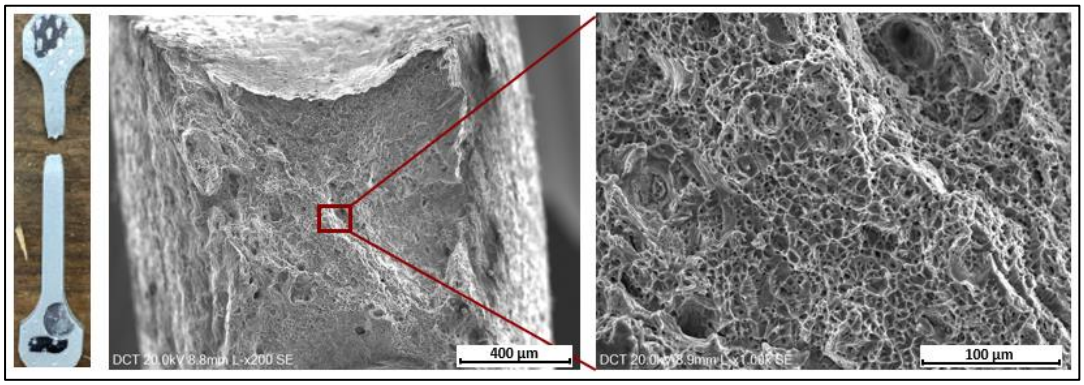

Figure 4.23 - Fracture surface of the sample FM3.

Comparing the fracture surface of the feeding material (FM3) and TBAR65-V-1, it was concluded that the additive material exhibits different elements, which accounts for the larger dimples, in contrast to the vertical specimen, which shows equiaxed and uniform dimples, as observed in Figure 4.21 and Figure 4.23. It is also noteworthy that, when comparing these two surfaces, the feeding material surface has a more spherical grain structure, while the TBAR65-V-1 shows a more parabolic grain structure. This may indicate that the latter was subjected to more complex stresses, possibly due to a denser surface resulting from the material processing.

All the specimens exhibit the 'necking' phenomenon in both horizontal and vertical directions, as well as in the TP9 and FM3 samples after the tensile test. The dimples are characteristic of ductile fracture, which subsequently indicates that all the specimens have high plasticity. It is therefore concluded that the fracture morphology is ductile, demonstrating high elongation in both horizontal and vertical specimens [28]. Additionally, the number of dimples in the horizontal direction is more than that in the vertical direction, which also verifies that the elongation in the horizontal direction is higher than that in the vertical direction, as expected, according to [2].
It was also concluded that the presence of particles in the FRAM tests did not affect the type of fracture obtained (Figure 4.22). It was noted that the specimens with particles did not fracture in the regions where the particles were present but rather due to natural fracture causes.

It was also possible to observe, in Figure 4.20, the distinction between the interlayer zone (transition zone) and the deposited layer zone. This difference is evident due to the rapid separation and breaking of interconnections in the transition zone, where the presence of dimples is noted around it due to the more refined grain. In the deposited layer zone, a tearing ridge is observed, as expected, according to [10]. This also leads to the conclusion that the vertical specimen may have fractured in the transition zone between layers.

4.3.4 Hardness Tests

In order to study the processed and non-processed zones, as well as the particle insertion zones, Vickers hardness tests were conducted on transverse sections of a sample with particles. Figure 4.24 presents the hardness map graphs obtained from the defined sample.

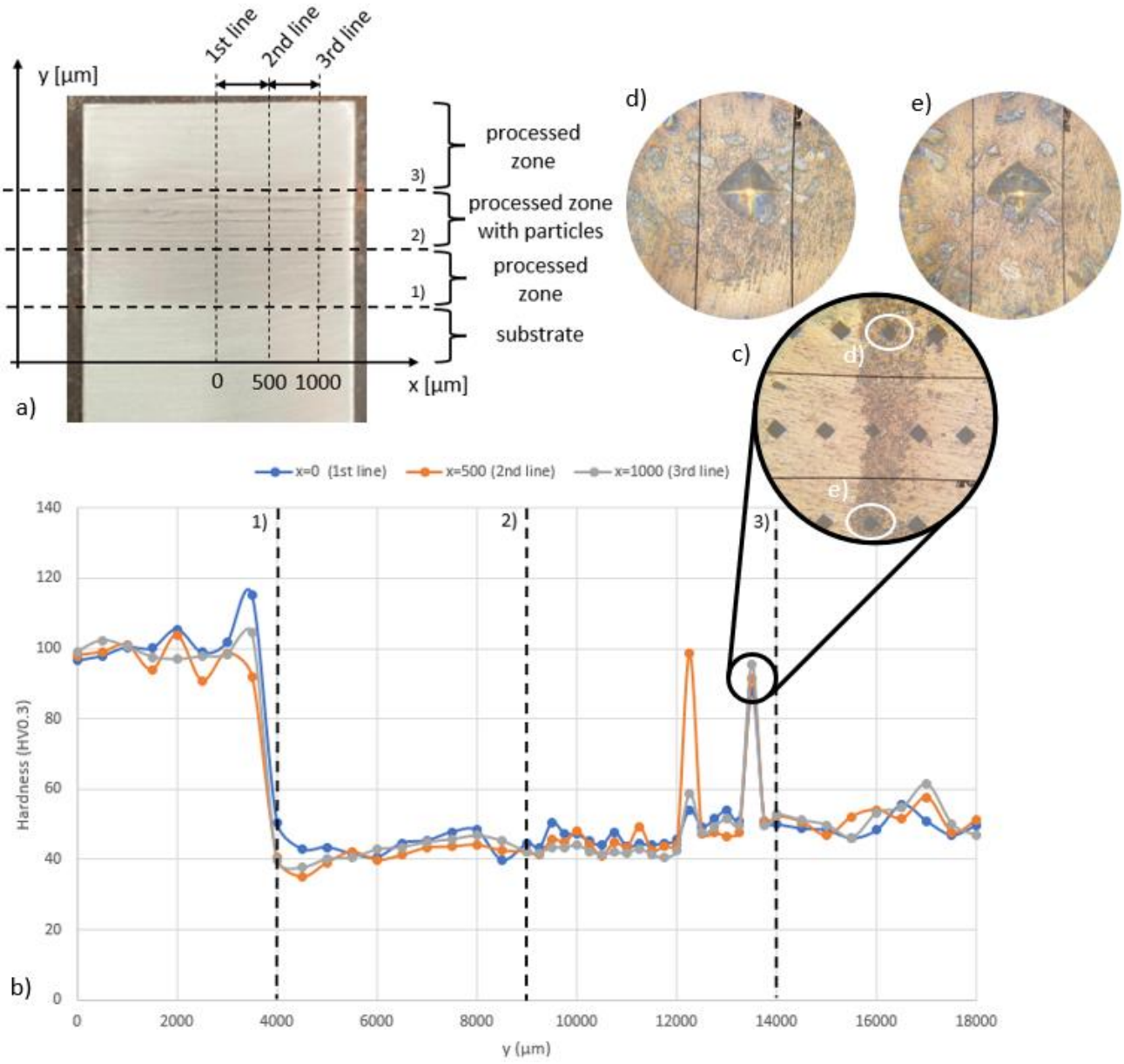

Figure 4.24- Hardness map performed on the transverse section of TP13 test: a) indentation schematic; b) results in a graph; c) transition zone with particles focusing on the indentations: d) 1st line; e) 3rd line.

By measuring the hardness of a sample, it is possible to observe changes in the material's resistance when processed.

Based on the results obtained, we can observe that in the substrate zone, up to line 1), the hardness remained relatively constant, averaging 100 HV0.3, which is expected given the hardness values for AA5083.

In the processed zone of the sample, between 1) and 2), there was an abrupt decrease in hardness values, averaging around 43 HV0.3. The difference in values between the substrate and the processed zone lies in the type of aluminum used, due to its chemical composition. It is possible to observe, in the transition zone between the first layer and the substrate (just before reaching line 1), a slight increase in hardness values, which explains the transition to a more processed material. In the layer itself, these values of 40-45 HV are observed, whereas for AA1000 alloys, the hardness values typically range from 25-35 HV. This increase is explained by the material having been processed, reducing the grain size and consequently increasing the hardness.

In the processed zone with particles, between 2) and 3), the average values did not increase significantly, but some sporadic oscillations were noted. Between 12000 μm and 14000 μm, two instances showed significant increases in hardness values, around 50-60 HV0.3. This is because, as observed in Figure 4.24 c), the indentations were performed in a transition zone between layers with a high concentration of particles, making it likely that the indentation was made on top of a particle.

Above the particle zone, up to line 3), stability in processed material values was observed again, approximately the same as in the substrate zone.

In conclusion, the presence of particles in the process did not significantly influence the resistance of the processed material and the produced wall.

5
CONCLUSION AND FUTURE WORKS

5.1 Conclusions

In this dissertation, multiple tests were conducted using the FRAM process, aiming to study, refine, and develop the process as well as its operational parameters. Several tests were performed with different types of feeding material geometries. Subsequently, tests were conducted incorporating ceramic particles, where different parameters influencing their incorporation were tested, along with the strategies and geometries used for layer deposition with particles.

This dissertation demonstrates that certain parameters must be met for successful layer deposition by FRAM, revealing some challenges. The production of walls with aluminum strips showed that layer deposition could lead to a relatively uniform surface when operational conditions are well controlled. It is necessary to ensure that the geometry of the feeding material does not exceed the defined parameters of the equipment used, as this is directly proportional to the efficient deposition of the feeding metal. The introduction of successive layers and programmed cooling pauses improved surface uniformity and quality, as evidenced by reduced roughness, comparing the results of the TBAR8 and TBAR65 tests, and improved interlayer adhesion. The insertion of ceramic particles was successful, showing good interlayer bonding in the particle zone, as well as particle dispersion within the material in the deposition area.

Regarding the influence of particle deposition in the FRAM process, it was concluded that a triangular cross-section profile with a cavity to accommodate the particles was necessary to provide some constraint but also some freedom for dispersion, preventing particle accumulation and subsequent poor particle bonding. However, the dispersion of particles within the layers was partial, and achieving a fully dispersed particle zone was not accomplished. The particles tended to concentrate in lines, without homogeneous dispersion, suggesting that further adjustments in the process are necessary to improve particle integration into the layers.

It was also concluded that particle dispersion in the processed material depends on the number of repeated passes over the particle layer, providing better mixing and subsequently better dispersion. This need for multiple passes showed that as the number of passes per layer increased, the already deposited wall tended to decrease in size due to layer flattening. Comparing zero repeated passes to two repeated passes, there was a 35% decrease in wall height for the TP12 test.

From uniaxial tensile tests and hardness tests, it was possible to conclude that the addition of particles did not affect the strength of the processed material, supporting the hypothesis that particle insertion still allowed interlayer bonding.

This was confirmed by hardness tests performed on a sample with zones with and without particles, showing a 10% variation in hardness values between these zones, highlighting the minimal difference. SEM analysis further confirmed that the tensile strength of samples with particles achieved UTS levels, on average, with a 1.1% decrease compared to samples without particles.

Through thermography, it was concluded that the highest temperature point during the process occurs when the tool is embedded in the substrate or the previous layer, making this the ideal point for the deformation of the feeding material. The temperatures reached during deposition range between 350 - 400ºC, which is the expected and ideal temperature for visco plastic deformation. It was also noteworthy that, in the tests conducted with particles, the temperatures reached in the processed zone were higher, causing the flattening of the already deposited layers and the overall flattening of the produced preform.

5.2 Future works

Using FRAM for the insertion of particles into a metallic component represented an innovative technological advancement and proved to yield very promising results. However, for future work, the following suggestions for improvement and new research focuses are presented for the development of this technology:

- The use of different metallographic analysis techniques, such as EDX, μ-CT or EBSD, could expand the horizons regarding the analysis of particles within the layers, their quantity, and their dispersion. The use of advanced characterization techniques can provide additional insights into the fracture mechanisms and stress distribution in the samples.
- Fatigue tests and electrical conductivity tests on specimens with and without particles would be of interest to study their behavior in different scenarios;
- The optimization of operational parameters should be continuously explored to improve the efficiency and quality of the produced samples;

- Further investigation into the influence of different types of particles and their concentrations in the FRAM process is recommended;
- Investigating different types of aluminum as feed material could open new possibilities for the FRAM process. Some aluminums with different chemical compositions and physical properties might offer significant improvements in the characteristics of the FRAM-produced walls. For instance, adding aluminum with varying silicon, copper, or magnesium content could alter the mechanical properties and corrosion resistance of the wall. Testing these different types of aluminum will allow identification of which compositions offer the best results for specific applications and contribute to formulating new materials with optimized performance;
- Previous experience demonstrated that the insertion of ceramic particles was successful, and exploring sensory particles could lead to new discoveries and innovations. These particles can provide additional properties such as increased wear resistance, improved thermal stability, or specific sensing capabilities. Conducting tests with different types of sensory particles will allow evaluation of their impact on the performance and functionality of the FRAM process and explore new potentially advantageous applications;

BIBLIOGRAPHY

[1] N. Tuncer and A. Bose, “Solid-State Metal Additive Manufacturing: A Review,” *JOM*, vol. 72, no. 9, pp. 3090–3111, Sep. 2020, doi: 10.1007/s11837-020-04260-y.

[2] R. Xie, Y. Shi, H. Liu, and S. Chen, “A novel friction and rolling based solid-state additive manufacturing method: Microstructure and mechanical properties evaluation,” *Mater Today Commun*, vol. 29, Dec. 2021, doi: 10.1016/j.mtcomm.2021.103005.

[3] J. P. Oliveira and T. G. Santos, “Demystifying ‘absolute truths’ of additive manufacturing,” *CIRP J Manuf Sci Technol*, vol. 54, pp. 57–62, Nov. 2024, doi: 10.1016/j.cirpj.2024.07.008.

[4] D. Herzog, V. Seyda, E. Wycisk, and C. Emmelmann, “Additive manufacturing of metals,” *Acta Mater*, vol. 117, pp. 371–392, Sep. 2016, doi: 10.1016/j.actamat.2016.07.019.

[5] W. M. Thomas, E. D. Nicholas, J. C. Needham, M. G. Murch, P. Temple-Smith, and C. J. Dawes, “Friction Welding, United States Patent,” 1995

[6] V. Gopan, K. Leo Dev Wins, and A. Surendran, “Innovative potential of additive friction stir deposition among current laser based metal additive manufacturing processes: A review,” Jan. 01, 2021, *Elsevier Ltd*. doi: 10.1016/j.cirpj.2020.12.004.

[7] A. Ardalanniya, S. Nourouzi, and H. Jamshidi Aval, “Fabrication of the laminated Al-Zn-Cup/Al-Zn composite using friction stir additive manufacturing,” *Mater Today Commun*, vol. 27, Jun. 2021, doi: 10.1016/j.mtcomm.2021.102268.

[8] M. Srivastava, S. Rathee, S. Maheshwari, A. Noor Siddiquee, and T. K. Kundra, "A Review on Recent Progress in Solid State Friction Based Metal Additive Manufacturing: Friction Stir Additive Techniques," Sep. 03, 2019, *Taylor and Francis Inc.* doi: 10.1080/10408436.2018.1490250.

[9] R. Xie, T. Liang, S. Chen, and H. Liu, "In-depth understanding of rotating toolhead-induced heat generation and material flow behavior in friction-rolling additive manufacturing," *Addit Manuf*, vol. 67, Apr. 2023, doi: 10.1016/j.addma.2023.103496.

[10] R. Xie, Y. Shi, R. Hou, H. Liu, and S. Chen, "Efficient depositing aluminum alloy using thick strips through severe deformation-based friction rolling additive manufacturing: processing, microstructure, and mechanical properties," *Journal of Materials Research and Technology*, vol. 24, pp. 3788–3801, May 2023, doi: 10.1016/j.jmrt.2023.04.075.

[11] H. Liu, Y. Xu, Y. Chen, R. Xie, and S. Chen, "Effects of toolhead size on the heat generation and material flow behaviors in solid state friction rolling additive manufacturing," *Journal of Materials Research and Technology*, vol. 28, pp. 1483–1496, Jan. 2024, doi: 10.1016/j.jmrt.2023.12.012.

[12] R. Xie, T. Liang, Y. Shi, and H. Liu, "Revealing the bonding mechanisms between deposit and substrate of the friction rolling additive manufactured hybrid aluminum alloys," *Addit Manuf*, vol. 56, Aug. 2022, doi: 10.1016/j.addma.2022.102942.

[13] R. Xie, X. Chen, Y. Shi, C. Yang, S. Chen, and H. Liu, "Printing high-strength high-elongation aluminum alloy using commercial ER2319 welding wires through deformation-based additive manufacturing," *Materials Science and Engineering: A*, vol. 868, Mar. 2023, doi: 10.1016/j.msea.2023.144773.

[14] H. Liu, Y. Sun, R. Xie, Y. Shi, Q. Shi, and S. Chen, "Continuous repair of groove damages using solid-state friction rolling additive manufacturing method," *Science and Technology of Welding and Joining*, vol. 28, no. 2, pp. 89–97, 2023, doi: 10.1080/13621718.2022.2117533.

[15] K. U. Kainer, *Metal matrix composites : custom-made materials for automotive and aerospace engineering*. Wiley-VCH, 2006.

[16] J. Qu, H. Xu, Z. Feng, D. A. Frederick, L. An, and H. Heinrich, "Improving the tribological characteristics of aluminum 6061 alloy by surface compositing with sub-micro-size ceramic particles via friction stir processing," *Wear*, vol. 271, no. 9–10, pp. 1940–1945, Jul. 2011, doi: 10.1016/j.wear.2010.11.046.

[17] A. T. Alpas and J. Zhang, "Effect of Microstructure (Particulate Size and Volume Fraction) and Counterface Material on the Sliding Wear Resistance of Particulate-Reinforced Aluminum Matrix Composites."

[18] I. Dinaharan, "Influence of ceramic particulate type on microstructure and tensile strength of aluminum matrix composites produced using friction stir processing," *Journal of Asian Ceramic Societies*, vol. 4, no. 2, pp. 209–218, Jun. 2016, doi: 10.1016/j.jascer.2016.04.002.

[19] F. Alves and F. Moreira, “PRODUÇÃO DE COMPÓSITOS BIMETÁLICOS REFORÇADOS COM MICROPARTÍCULAS FUNCIONAIS POR UPWARD FRICTION STIR PROCESSING (UFSP).”

[20] P. M. Ferreira, M. A. Machado, M. S. Carvalho, and C. Vidal, “Granting Sensorial Properties to Metal Parts through Friction Stir Processing,” *Measurement (Lond)*, vol. 207, Feb. 2023, doi: 10.1016/j.measurement.2022.112405.

[21] P. M. Ferreira, A. Meireles, C. Vidal, M. S. Carvalho, and M. A. Machado, “Evaluation of self-sensing material behaviour: Insights from cyclic and pulse load testing,” *Measurement (Lond)*, vol. 234, Jul. 2024, doi: 10.1016/j.measurement.2024.114878.

[22] P. M. Ferreira *et al.*, “Self-sensing metallic material based on PZT particles produced by friction stir processing envisaging structural health monitoring applications,” *Mater Charact*, vol. 205, Nov. 2023, doi: 10.1016/j.matchar.2023.113371.

[23] P. M. Ferreira *et al.*, “Smart piezoelectric composite: impact of piezoelectric ceramic microparticles embedded in heat-treated 7075-T651 aluminium alloy,” *International Journal of Mechanics and Materials in Design*, 2024, doi: 10.1007/s10999-024-09731-7.

[24] P. M. Ferreira *et al.*, “Enabling electrical response through piezoelectric particle integration in AA2017-T451 aluminium parts using FSP technology,” *Smart Mater Struct*, vol. 33, no. 6, Jun. 2024, doi: 10.1088/1361-665X/ad4d45.

[25] I. Milosan *et al.*, “Characterization of aluminum alloy-silicon carbide functionally graded materials developed by centrifugal casting process,” *Applied Sciences (Switzerland)*, vol. 11, no. 4, pp. 1–14, Feb. 2021, doi: 10.3390/app11041625.

[26] J. David Fernandes Caçador, “Sensorial properties assessment in metallic parts with piezoelectric particles.”

[27] K. Anderson-Wedge *et al.*, “Characterization of the fatigue behavior of additive friction stir-deposition AA2219,” *Int J Fatigue*, vol. 142, Jan. 2021, doi: 10.1016/j.ijfatigue.2020.105951.

[28] C. Du, Q. Pan, S. Chen, and S. Tian, “Effect of rolling on the microstructure and mechanical properties of 6061-T6 DS-FSW plate,” *Materials Science and Engineering: A*, vol. 772, Jan. 2020, doi: 10.1016/j.msea.2019.138692.

A

APPENDIX – TECHNICAL DRAWINGS

A.1 Technical drawing of Plate 1 + Plate 2 (horizontal plate of the guiding system

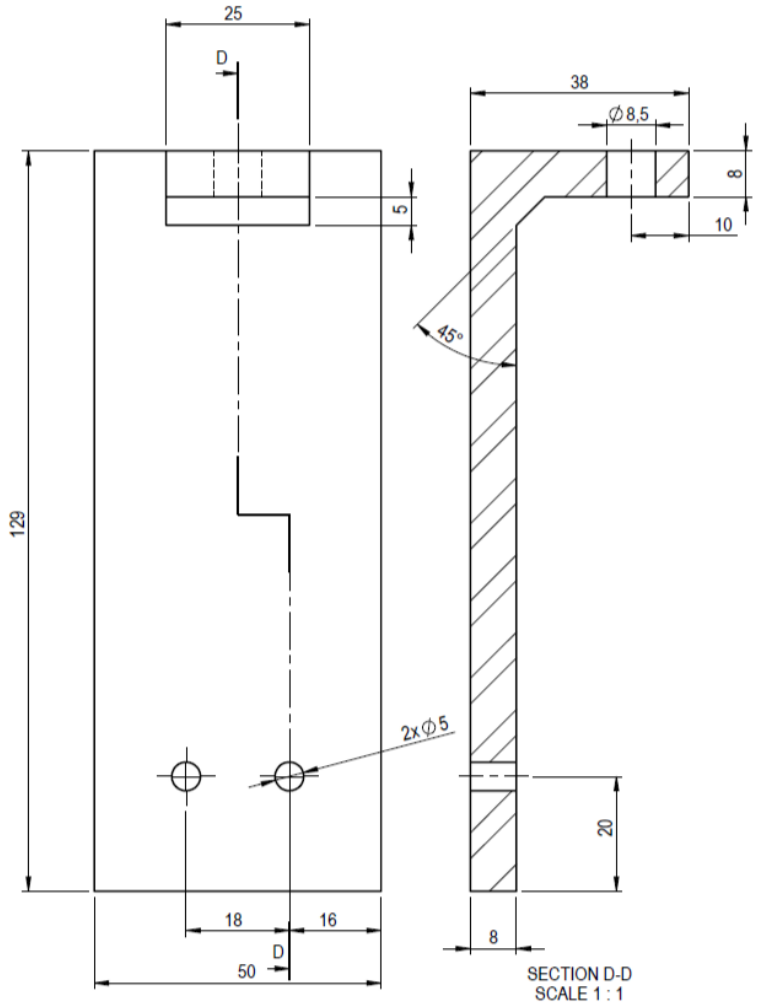

Figure A.1 - Technical drawing of Plate 1 and Plate 2 (horizontal plate of the guiding system)

A.2 Technical drawing of Plate 3 (vertical plate of the guiding system)

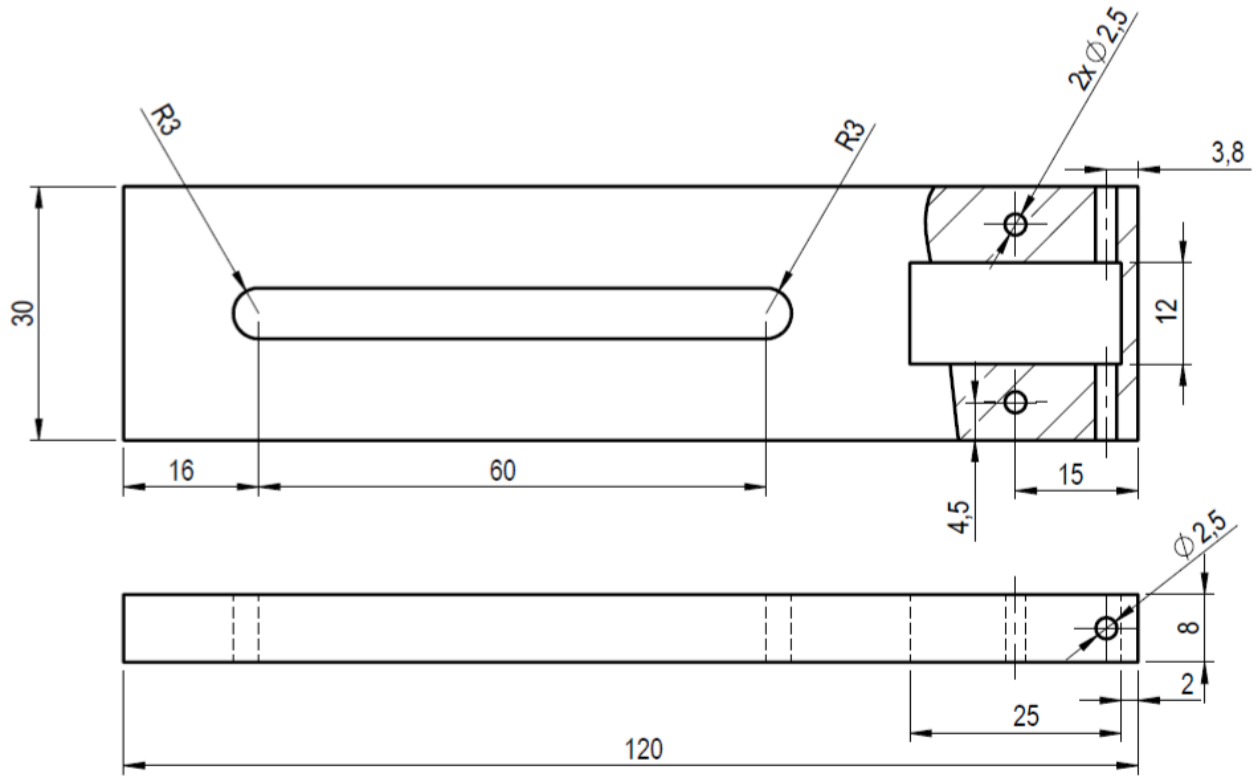

Figure A.2 - Technical drawing of Plate 3 (vertical plate of the guiding system).

A.3 Technical drawing of Plate 4 (aluminum plate for guiding the feeding material)

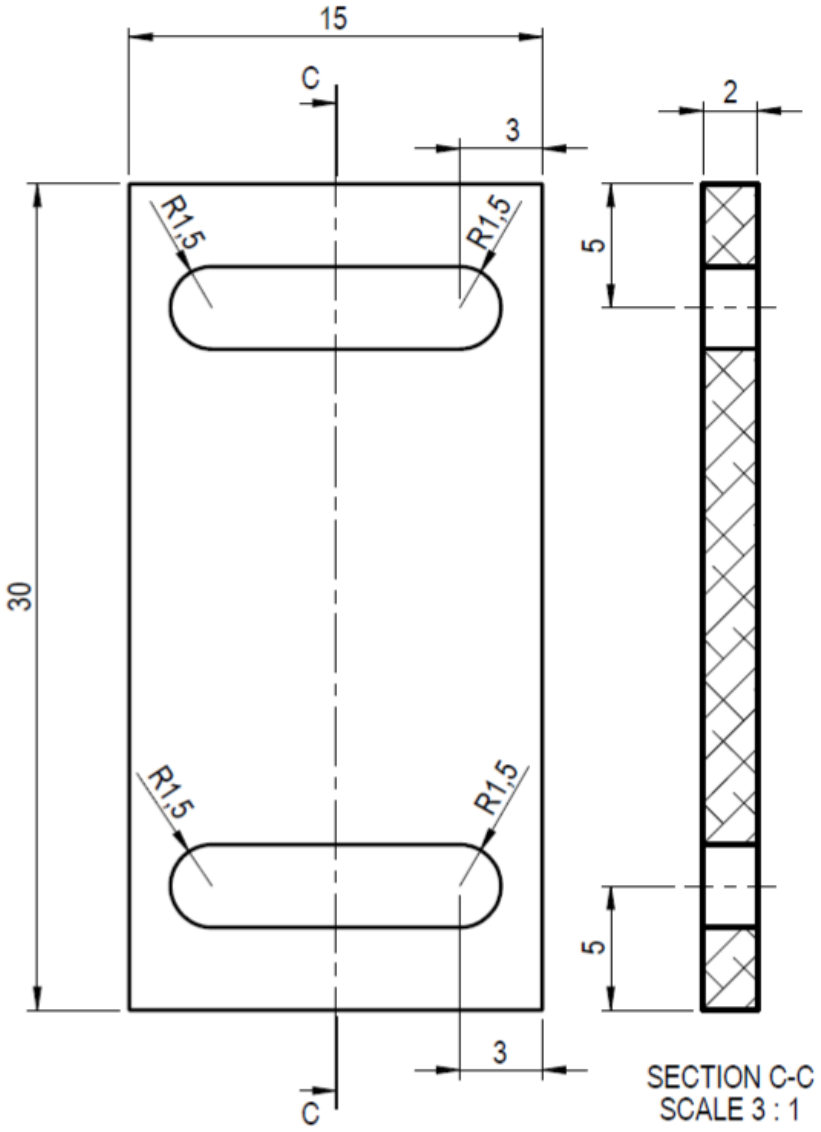

Figure A.3 - Technical drawing of Plate 4 (aluminum plate for guiding the feeding material)

A.4 Technical drawing of the tool used in the production of walls by FRAM

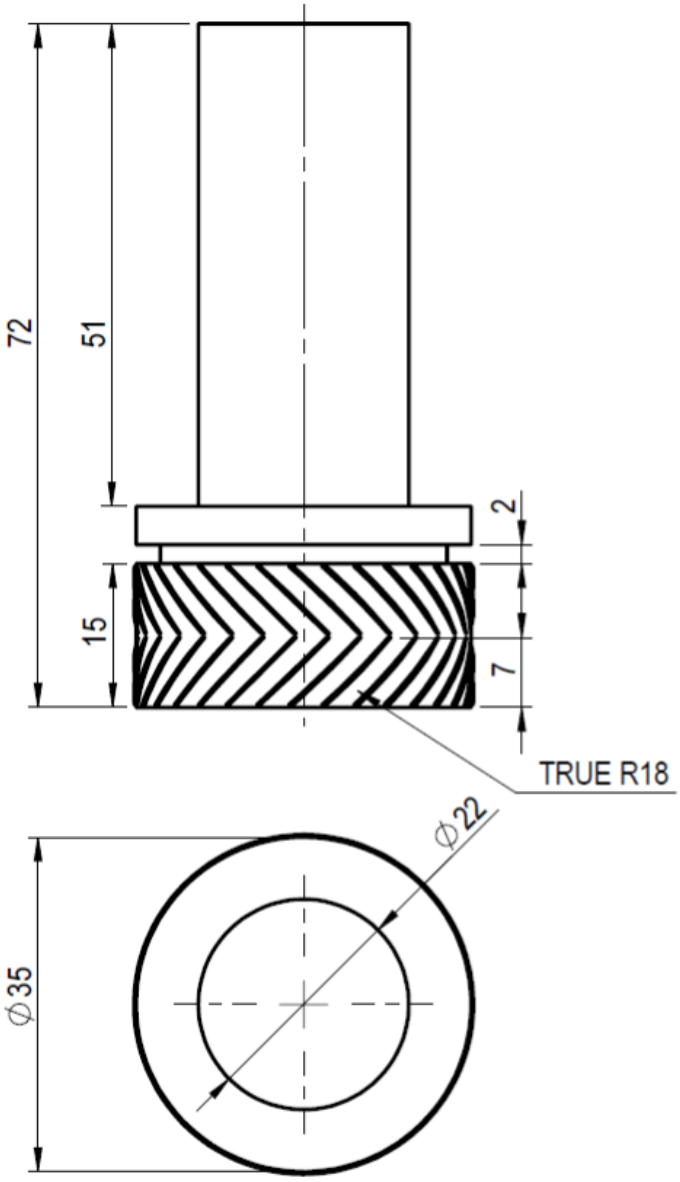

Figure A.4 - Technical drawing of the tool used in the production of walls by FRAM.

B

PRODUCTION AND EXPERIMENTAL PROCEDURES

B.1 Procedures for the production of the guiding system

Table B.1 - Set of procedures for producing each component of the guiding system

Part	Process	Tools	Description
Plate 1 (attached to the milling machine)	Drilling	Drill Φ 6,5 mm	Through hole
Plate 2 (horizontal)	Drilling Tap Thread	Drill Φ 5 mm Tap M6	Two through holes equally spaced from the sides
Plate 3 (vertical)	Drilling Roughing	Drill Φ 6mm Cutter Φ 6mm	Two holes, at the beginning and end of the slot, and milling operation to open the slot
	Drilling Roughing	Drill Φ 6mm Cutter Φ 4mm	Drill a hole in the center of the rectangular slot and use a milling cutter to open it
	-	Tap M6	Opening Thread
	Drilling	Drill Φ 4mm Drill Φ 3mm Tap M4 Tap M3	Drill holes above and below the rectangular slot and thread them Drill holes at the top and bottom of the plate and tap them